FACTORS WHICH INFLUENCE THE SIGNAL-TO-NOISE RATIO IN ATOMIC EMISSION FLAME SPECTROMETRY

By

LLOYD DEAN REMINGTON

A DISSERTATION PRESENTED TO THE GRADUATE COUNCIL OF
THE UNIVERSITY OF FLORIDA
IN PARTIAL FULFILLMENT OF THE REQUIREMENTS FOR THE
DEGREE OF DOCTOR OF PHILOSOPHY

UNIVERSITY OF FLORIDA

April, 1966

ACKNOWLEDGMENTS

I wish to gratefully acknowledge the enthusiasm, advice and friendship of Dr. J. D. Winefordner in preparing this dissertation and also the assistance of Dr. L. A. Arnold, Dr. W. S. Brey, Dr. W. M. Jones, Dr. R. C. Stoufer, and Dr. T. J. Vickers. Without the cheerful patience and support of my wife and daughters, and the financial help of the National Science Foundation through various Institutes and Fellowships, the following study could not have been accomplished.

TABLE OF CONTENTS

Page

ACKNOWLEDGMENTS ii

LIST OF TABLES. v

LIST OF FIGURES viii

KEY TO SYMBOLS. ix

Section

I. INTRODUCTION. 1

II. INSTRUMENTATION 4

III. THEORY. 6

IV. EXPERIMENTAL MEASUREMENTS 34

A. Measurement of Parameter Values. 34

1. Photoanodic dark current values, i_d . . 36

2. Photosensitivity factor values, γ . . . 37

3. Photomultiplier tube gain values, M . . 39

4. Continuum intensity values, I_c. 41

5. Flame flicker parameter values, ψ . . . 45

6. Frequency response band width values, $\overline{\Delta i}_e \sqrt{\Delta f}$ and $\overline{\Delta i}_p$ 47

7. Electrometer and photomultiplier tube noise values, $\overline{\Delta i}_e$ and $\overline{\Delta i}_p$ 51

B. Method of Obtaining and Evaluating Experimental Measurements of Signal-to-Noise Ratio. 53

C. Comparison of the Theoretical and Experimental Plots of Signal-to-Noise Ratio Versus Slit Width 60

Section Page

V. INFLUENCE ON SIGNAL-TO-NOISE RATIO VERSUS SLIT WIDTH CURVES OF INDEPENDENTLY VARYING INDIVIDUAL PARAMETERS 83

VI. SUMMARY OF CONCLUSIONS 93

APPENDICES. 95

LITERATURE CITED. 136

BIOGRAPHICAL SKETCH 139

LIST OF TABLES

Table Page

1. Dissociation Constants of the Chloride, Monoxide, Monohydride, and Monohydroxide Species, and the Ionization Constants, for Sodium at Several Temperatures 17

2. Dissociation Constants of the Chloride, Monoxide, Monohydride, and Monohydroxide Species, and the Ionization Constants, for Lithium at Several Temperatures. 18

3. Dissociation Constants of the Chloride, Monoxide, Monohydride Species, and the Ionization Constants, for Barium at Several Temperatures 19

4. Dissociation Constants of the Chloride, Monoxide, Monohydride Species, and the Ionization Constants, for Calcium at Several Temperatures 20

5. Dissociation Constants of the Chloride, Monoxide, Monohydride Species, and the Ionization Constants, for Strontium at Several Temperatures 21

6. Partial Pressures of the Atomic Species of Oxygen and Hydrogen, and the Neutral Hydroxide Species, in the Flame Gases of Several Flames 23

7. N Values for Sodium in Three Flames Calculated With, and Without, Consideration of the Monoxide and Monohydride Species 26

8. N Values for Lithium in Three Flames Calculated With, and Without, Consideration of the Monoxide and Monohydride Species 27

9. Measured Voltage Between the Cathode and Ground and Cathode and Anode of the Photomultiplier on the Beckman DU Spectrophotometer at Several Sensitivity Settings 35

Table Page

10. Measured Photoanodic Dark Current Values at Several Voltages Applied to the Photomultiplier Tube 38

11. Measured Values of the Photosensitivity Factor at Several Wavelengths 40

12. Flame Continuum Intensity Values, Obtained by Two Methods of Measurement and One Literature Source, at Five Wavelengths in Three Flame Types. 46

13. Measured Values of the Signal-to-Noise Ratio at High Concentrations for the Calculation of Flame Flicker Factor Values. 48

14. Calculated and Measured Signal-to-Noise Ratio for Three Concentrations of Barium in a Stoichiometric Hydrogen-Oxygen Flame 61

15. Calculated and Measured Signal-to-Noise Ratios for Three Concentrations of Barium in a Fuel Rich Hydrogen-Oxygen Flame 62

16. Calculated and Measured Signal-to-Noise Ratios for Three Concentrations of Barium in a Stoichiometric Acetylene-Oxygen Flame. . . . 63

17. Calculated and Measured Signal-to-Noise Ratios for Three Concentrations of Calcium in a Stoichiometric Hydrogen-Oxygen Flame 64

18. Calculated and Measured Signal-to-Noise Ratios for Three Concentrations of Calcium in a Fuel Rich Hydrogen-Oxygen Flame. 65

19. Calculated and Measured Signal-to-Noise Ratios for Three Concentrations of Calcium in a Stoichiometric Acetylene-Oxygen Flame. . . . 66

20. Calculated and Measured Signal-to-Noise Ratios for Three Concentrations of Lithium in a Stoichiometric Hydrogen-Oxygen Flame 67

21. Calculated and Measured Signal-to-Noise Ratios for Three Concentrations of Lithium in a Fuel Rich Hydrogen-Oxygen Flame. 68

Table Page

22. Calculated and Measured Signal-to-Noise Ratios for Three Concentrations of Lithium in a Stoichiometric Acetylene-Oxygen Flame 69

23. Calculated and Measured Signal-to-Noise Ratios for Three Concentrations of Sodium in a Stoichiometric Hydrogen-Oxygen Flame. 70

24. Calculated and Measured Signal-to-Noise Ratios for Three Concentrations of Sodium in a Fuel Rich Hydrogen-Oxygen Flame. 71

25. Calculated and Measured Signal-to-Noise Ratios for Three Concentrations of Sodium in a Stoichiometric Acetylene-Oxygen Flame 72

26. Calculated and Measured Signal-to-Noise Ratios for Three Concentrations of Strontium in a Stoichiometric Hydrogen-Oxygen Flame. 73

27. Calculated and Measured Signal-to-Noise Ratios for Three Concentrations of Strontium in a Fuel Rich Hydrogen-Oxygen Flame 74

28. Calculated and Measured Signal-to-Noise Ratios for Three Concentrations of Strontium in a Stoichiometric Acetylene-Oxygen Flame 75

LIST OF FIGURES

Figure Page

1. Typical chart readout, with interpretation, for measurement of signal and noise 57

2. Comparison of theoretical and experimental signal-to-noise ratio versus slit width curves for a 0.1 ppm sodium (5890 Å) solution in a stoichiometric acetylene-oxygen flame. 79

3. Comparison of theoretical and experimental signal-to-noise ratio versus slit width curves for a 1000 ppm lithium (6708 Å) solution in a stoichiometric acetylene-oxygen flame. 80

4. Comparison of theoretical and experimental signal-to-noise ratio versus slit width curves for a 10 ppm calcium (4227 Å) solution in a fuel rich hydrogen-oxygen flame. 81

5. Signal-to-noise ratio versus slit width curves for extreme values of the flame flicker factor. 85

6. Signal-to-noise ratio versus slit width curves for extreme values of the continuum intensity 86

7. Signal-to-noise ratio versus slit width curves for extreme values of the minimum resolving power slit width. 87

8. Signal-to-noise ratio versus slit width curves for extreme values of the photosensitivity factor and the photomultiplier tube gain factor. 88

9. Signal-to-noise ratio versus slit width curves for extreme values of the photoanodic dark current 89

KEY TO SYMBOLS

A	area of collimator, cm^2
A_t	transition probability, sec^{-1}
a	damping constant, no units
B	factor characteristic of photodetector surface, no units
$B(T)$	partition function, no units
C	concentration, moles $liter^{-1}$
c	speed of light, 3×10^{10} cm sec^{-1}
E_u	excitation energy of state u, electron volts
exp	natural log base, e, raised to the power of --
e_c	electronic charge, 1.6×10^{-19} coulombs
F	focal length of collimator, cm
Δf	frequency interval over which the amplifier-readout system responds, sec^{-1}
G	gain per stage of the photodetector, no units
g_u	statistical weight of upper u state, no units
H	height of slit opening, cm
h	Planck's constant, 6.6×10^{-27} erg-sec
I	integrated intensity of the thermally emitted spectral line, watts cm^{-2} $ster^{-1}$
i	photoanodic signal due to emitted intensity, I, amperes
I_c	intensity of the flame continuum, watts cm^{-2} $ster^{-1}$ $m\mu^{-1}$
I_{cw}	measured intensity of thermal emission of the flame when only distilled water is being aspirated into it, watts cm^{-2} $ster^{-1}$

i_c	signal due to emitted intensity, I_c, amperes
i_d	photoanodic dark current of the photodetector, amperes
i_s	photoanodic signal due to emitted intensity, I, when a solution of metal ions is being aspirated into the flame, amperes
i_w	photoanodic signal due to emitted intensity, I_{cw}, amperes
$\overline{\Delta I}$	r.m.s. fluctuation in I, watts cm^{-2} $ster^{-1}$ $sec^{-1/2}$
$\overline{\Delta I}_c$	r.m.s. fluctuation in I_c, watts cm^{-2} $ster^{-1}$ $m\mu^{-1}$ $sec^{-1/2}$
$\overline{\Delta i}_c$	r.m.s. noise (photoanodic) signal due to the flame continuum, amperes
$\overline{\Delta i}_e$	r.m.s. noise (photoanodic) signal due to the electrometer, amperes
$\overline{\Delta i}_p$	r.m.s. noise (photoanodic) signal due to the phototube, amperes
$\overline{\Delta i}$	r.m.s. noise (photoanodic) due to thermal emission, amperes
$\overline{\Delta i}_T$	r.m.s. noise (photoanodic) signal, amperes
K_1	dissociation constant for the metal chloride salt, atm^2 for alkaline earths; atm for alkali metals
K_2	dissociation constant for the metal monoxide, atm
K_3	dissociation constant for the metal monohydride, atm
K_4	dissociation constant for the metal monohydroxide, atm
K_5	ionization constant of the metal, atm
[illegible]	Boltzmann constant (for units see text)
K_c	γT_f H (A/F^2)
K_d	2 e_c BM
k°	atomic absorption coefficient at line center, cm^{-1}
L	diameter of the flame, cm

ln	natural log
M	amplification factor of photodetector, no units
M_a	atomic weight, atomic mass units
N	total atomic concentration of metal of interest, atoms cm^{-3}
N_i	atomic concentration, in flame gases, corresponding to the intersection of the extensions of the two linear portions of the analytical curve, atoms cm^{-3}
n	entrance optics factor, no units
N_T N_{298}	moles present at temperature T and temperature 298° K, respectively
P_{Cl}	partial pressure of atomic chlorine in the flame gases, atm
P_e	total partial pressure of electrons in the flame gases, atm
P'_e	partial pressure of electrons, in the flame gases, due only to ionization of the flame gas molecules, atm
P_H	partial pressure of atomic hydrogen in the flame gases, atm
P_M	partial pressure of the atomic metal species in the flame gases, atm
$P_M{}^+$	partial pressure due to the metal ion present in the flame gases, atm
P_{MCl}	partial pressure due to alkali metal chloride in flame gases, atm
P_{MCl_2}	partial pressure due to the alkaline earth metal chloride in the flame gases, atm
P_{MH}	partial pressure due to the metal monohydride in the flame gases, atm
P_{MO}	partial pressure due to the metal monoxide in the flame gases, atm

P_{MOH}	partial pressure due to the metal monohydroxide present in the flame gases, atm
P_T	total partial pressure of the metal of interest in all of its forms, atm
Q	flow rate of unburned gases, cm^3 sec^{-1}
R_d	reciprocal linear dispersion, mμ cm^{-1}
s	spectral band width, mμ
s_c	spectral band width due to abberations and diffraction limit, mμ
s_m	spectral band width as determined by the mechanical slit width, mμ
T	absolute flame temperature, °K
T_f	transmission factor, no units
W	slit width, cm
W_o	optimum slit width, cm
W_m	minimum resolving power slit width, cm
γ	photosensitivity factor, amperes $watt^{-1}$
δ	factor to account for line broadening other than Doppler broadening, no units
ϵ	efficiency of atomization, no units
ζ	term to account for non-alignment of slit center and spectral line, no units
λ_o	wave length at spectral line center, cm
ν_o	frequency at spectral line center, sec^{-1}
$\Delta\nu_D$	Doppler half width of a line, sec^{-1}
ξ	$\overline{\Delta I_c / I_c}$, $sec^{-1/2}$

π	3.14, no units
Φ	aspiration rate of solution, cm^3 min^{-1}
ψ	$\overline{\Delta I}/I$, $sec^{-1/2}$

I. INTRODUCTION

This research is a continuation of a long-range effort being made in this laboratory[26,27,28,30,31,32] to provide a sound theoretical explanation for all of the processes which occur in flame spectrometry from the time a sample solution is aspirated into the flame until a signal is read out. Because the present work is limited to atomic emission flame spectrometry the following brief review will deal only with that phase of flame spectrometry. Winefordner[26] has studied the relation between spectrometer slit width and measured intensity; Winefordner, Mansfield, and Vickers[27,28] have measured the temperatures in various analytical flames and the efficiency of atomization of the sample solution into analytical flames; Winefordner and Vickers[30] gave a method of calculating the limit of detectability in atomic emission flame spectrometry; Winefordner and Veillon[31] studied the effect of electrometer noise on the limit of detectability; and Winefordner, Vickers, and Remington[32] described a way to calculate that particular concentration of the atomic metal species in the flame gases at which self-absorption of the emitted light is sufficient to change the slope of the analytical working curve. Of course there are other workers than those of this laboratory who are interested in this area and have published considerable material relating directly to it. Alkemade,[1,8] Broderson,[2,3] Mavrodineanu and Boiteux,[20] Gilbert,[7] Gaydon,[6] Sugden,[13,15] have written articles of theoretical value.

The major contributions of this dissertation to a more complete understanding of the choice of optimum conditions for flame emission spectrometry are: (a) those instrumental, flame, and solution conditions which produce the largest values of the signal-to-noise ratio also represent the optimum working conditions; (b) the signal-to-noise ratio expressions presented by Winefordner and Vickers[30] have been altered to consider the electrometer noise[31] and the minimum resolving power slit width[8] and to consider higher concentrations of sample solution than exist at the limit of detection; (c) experimental measurements of the values of various instrumental parameters used in the theoretical calculation of the signal-to-noise ratio have been made; (d) the optimum monochromator slit width for various experimental conditions was obtained by calculating and experimentally measuring the effect of slit width on the signal-to-noise ratio. This was done by calculating the optimum slit width from a derived equation and also by the graphical plots of calculated and experimentally measured signal-to-noise ratios against slit width. This plot showed, not only the size of the optimum slit width, but also the sensitivity of the measurement to variation in slit width; (e) verification of the derived expressions used by comparing experimentally measured and theoretically calculated values of signal-to-noise ratio, and also by comparing the experimentally measured and theoretically calculated shapes of the signal-to-noise ratio versus slit width curves; (f) a study of the effect of variations of instrument, flame, and solution parameters on the signal-to-noise ratio versus slit width curve; (g) because the theoretical calculations are tedious and time consuming, Fortran programs were prepared to obtain the calculated values of signal-to-noise ratios for various instrument, flame, and solution parameters.

II. INSTRUMENTATION

The apparatus used in this study included a Beckman DU spectrophotometer (Beckman Instruments Inc., Fullerton, California) with a flame attachment; a DU power supply unit, and an externally attached readout system with meter or recorder; also a Jarrell-Ash 0.5 meter Ebert mounted grating mounted grating monochromator (Jarrell-Ash Co., Newtonville, Mass.) using an ac amplifier system[17] and a 10 mv Sargent (Model TR) recorder (E. H. Sargent & Co., 4647 West Foster Ave., Chicago, Ill. 60630). The amplifier of the Beckman DU was arranged so that the output signal could be fed into (a) the regular readout system; (b) into an external ammeter, or (c) into a Heathkit EUW-20A Servo Recorder (Heath Co., Benton Harbor, Michigan). The system containing the external ammeter also contained a helipot zero-suppress circuit with a 1000 unit scale and 1-1/2 volt battery. The mirror in the flame attachment housing was covered during the measurements so that the monochromator would not collect reflected light emitted by the flame. (In this way the area of the collecting lens or mirror, A, divided by the square of the focal length of the lens or mirror, F, would be an accurate measure of the number of steradians (solid angles) of light from the flame that enter the monochromator.) The condenser in parallel with the phototube load resistor which established the frequency response band width value (Δf) of the amplifier-readout system for the DU was disconnected for this study.

The same 1P28 photomultiplier tube that was used on the DU was also used when studies on the Jarrell-Ash monochromator were carried out. The Jarrell-Ash electrometer amplifier high voltage power supply (Model 26-770) was used for these measurements. The electrometer-recorder combination also provided a direct means of obtaining the photoanodic current in amperes. A calibrated Eppley Laboratory (Newport, R.I.) standard light source was used to measure absolute intensities of the flame background. The spectral radiance in microwatts mm^{-2} $ster^{-1}$ $m\mu^{-1}$ of this source was known at intervals of 10 mu over the wave length range of 250 mu to 750 mu. These values were converted to watts cm^{-2} $ster^{-1}$ $m\mu^{-1}$ for the purposes of this study.

III. THEORY

The basic expression for the photoanodic signal in amperes in atomic emission flame spectrometry, as derived by Winefordner and Vickers[30] is

$$i = \kappa \gamma T_f IWH(A/F^2)n \quad , \qquad (1)$$

where κ[30] is a term to account for the possibility that the monochromator may not be set exactly at the wavelength of the emitted spectral line. This is of importance when the spectral line of interest is a multiplet which cannot be resolved by the monochromator. In the case of a single, sharp, isolated spectral line, with the monochromator set at the line center, the value of κ is unity. In this study, κ is experimentally made to be unity. The parameter γ is the photosensitivity factor; that is, the current in amperes produced at the anode of the detector for each watt of radiant power striking the photocathode. The term T_f is the transmission factor which accounts for the loss of emitted light, due to reflection from the lenses, etc., within the monochromator, and I is the total radiant intensity (integrated intensity) in watts cm^{-2} $ster^{-1}$ of the emitted spectral line. The parameters W and H are the width and height, respectively, in cm of the monochromator slit opening, and A/F^2 is the number of steradians viewed by the spectrometric system as long as the effective slit aperture is filled with radiation. The parameter n[30] accounts for more than one multiple of the solid angle A/F^2 being focused on the slit aperture by the use of suitable entrance optics. In the experimental work done here, the mirror in the flame housing of the Beckman DU was blocked off, and so the value of n in the theoretical treatment is assumed to be unity.

In order to use Equation (1), it is necessary to make certain assumptions. A complete listing of these assumptions is: (a) $\gamma = 1$; (b) $n = 1$; (c) the entrance optics are sufficiently well aligned so as to assure that the radiation entering the monochromator completely fills the collimator, and (d) entrance and exit slits are the same size. For the experimental system used in this study, these four assumptions are valid (see above discussion).

The equation given by Winefordner and Vickers[30] for the total root-mean-square (r.m.s.) fluctuation (photoanodic) current, Δi_T, is

$$\overline{\Delta i}_T = (\overline{\Delta i}_p{}^2 + \overline{\Delta i}_c{}^2 + \overline{\Delta i}_e{}^2 \, \Delta f)^{1/2} \quad , \qquad (2)$$

where $\overline{\Delta i}_c$ is the r.m.s. noise (photoanodic) signal due to flame background flicker, $\overline{\Delta i}_p$ is the phototube noise, and $\overline{\Delta i}_e \sqrt{\Delta f}$ is the electrometer r.m.s. (photoanodic) noise signal. Because $\overline{\Delta i}_c$, $\overline{\Delta i}_p$ and $\overline{\Delta i}_E \sqrt{\Delta f}$ are independent noise signals, they are added quadratically. In the expression used by Winefordner and Vickers[30] for $\overline{\Delta i}_p$, it is assumed that only the shot effect noise, which depends on the photoanodic dark current through the phototube, is significant; that is, Johnson noise due to random electron motion in the phototube load resistor is negligible. Also for the studies in this dissertation the electrometer noise $\overline{\Delta i}_e \Delta f^{1/2}$ is found to be negligible (see Section IV A.7) compared to $\overline{\Delta i}_p$ and $\overline{\Delta i}_c$. The phototube noise current, Δi_p, is

$$\overline{\Delta i}_p = [2e_c\ BM\ \Delta f(i_d+i_c)]^{1/2} \quad , \tag{3}$$

where e_c is the charge on an electron in coulombs, B is a constant approximately equal to $1 + 1/G + 1/G^2$.....(where G is the gain per stage of the photomultiplier tube), M is the total amplification factor of the photomultiplier tube, Δf is the frequency response band width in sec^{-1} of the amplifier-readout circuit; i_d is the photoanodic dark current in amperes, and i_c is the photoanodic signal in amperes produced by the intensity of the flame continuum. The continuum signal, i_c, is given by

$$i_c = \gamma T_f I_c\ s\ WH(A/F^2) \quad , \tag{4}$$

where s is the spectral band width in mμ, and I_c is the watts cm^{-2} $ster^{-1}$ (or steradiancy) per mμ of spectral band width of the continuum. Therefore, $I_c s$ is the total steradiancy of the continuum that enters the instrument. The expression used for $\overline{\Delta i}_c$ is

$$\overline{\Delta i}_c = \gamma T_f \overline{\Delta I}_c \, s \, WH(A/F^2)\Delta f^{1/2} \quad , \qquad (5)$$

where $\overline{\Delta I}_c$ is the r.m.s. fluctuation in the steradiancy (or noise) per mμ of spectral band width of the continuum, and therefore $\overline{\Delta I}_c s$ would be the total r.m.s. noise due to the continuum flicker entering the instrument. The total noise, $\overline{\Delta i}_T$, is therefore given[30] by

$$\overline{\Delta i}_T = [2e_c BM\Delta f(i_d + \gamma T_f WH(A/F^2)I_c s) + \{\gamma T_f WH(A/F^2)\Delta I_c s\}^2 \Delta f]^{1/2} \; . \qquad (6)$$

The assumptions involved here include those mentioned earlier concerning Equation (1) and also the following assumptions. The signal due to the emitted light from the metal atoms in the sample near the limit of detection is not significant, and there is no significant noise contribution from either the electrometer noise or the thermal emission flicker.

However the study is not limited to the very low sample concentrations near the limit of detection, and so a noise contribution from the r.m.s. fluctuations of the sample thermal emission must be included, that is, $\overline{\Delta i}$. This fluctuation is caused in the same way as the fluctuations in the continuum intensity and therefore cannot be treated as a source of noise that is independent of $\overline{\Delta i}_c$; that is, noise signals $\overline{\Delta i}$ and $\overline{\Delta i}_c$ add linearly. Winefordner and Vickers[30] discussed the linear addition of dependent noises and the quadratic addition of noises which are independent of each other.

The spectral band width, s, is approximately equal to the sum of two terms;[30] one, s_m, which is equal to the reciprocal linear dispersion, R_d, multiplied by the slit width (W) in cm and also a constant term, s_c, which is equal to reciprocal linear dispersion, R_d, multiplied by a constant slit width (W_m) in cm. Thus

$$s = s_m + s_c = R_d(W + W_m) \qquad (7)$$

The minimum resolving power slit width, W_m, represents the minimum width to which the slits can be closed and still maintain a properly focused image on the dispersing element. The minimum resolving power slit width, W_m is due to: (a) the improper focus of optics within the instrument leading to an inescapable aberration or fuzziness; (b) diffraction effects at an infinitely narrow slit width (i.e., the slit at very narrow widths acts as a transmission diffraction grating).

Therefore Equation (6), with the assumptions and inclusions mentioned above, is then given more exactly by

$$\overline{\Delta i}_T = [2e_c BM\Delta f \left\{ i_d + \gamma T_f WH(A/F^2)[I_c R_d(W+W_m)+I] \right\} +$$

$$\left\{ \gamma T_f WH(A/F^2)[\overline{\Delta I}_c R_d(W+W_m)+\overline{\Delta I}] \right\}^2 \Delta f]^{1/2} \quad . \qquad (8)$$

Equation (8) can be simplified by combining the constant terms and substituting

$$K_d = 2e_c BM \quad , \qquad (9)$$

and

$$K_c = \gamma T_f H(A/F^2) \quad . \qquad (10)$$

The terms $\overline{\Delta I}$ and $\overline{\Delta I}_c$ can be further simplified. Equation (1) shows that the signal, i, is directly proportional to the intensity I; consequently, fluctuations in I, $\overline{\Delta I}$, produce fluctuations in i, $\overline{\Delta i}$, or noise. Fluctuations in I are amplified to the same degree that I itself is amplified. Consequently, if the fluctuations of I produce a steady "white" noise superimposed on a steady dc signal, the ratio of r.m.s. noise-to-signal should remain constant at various states of amplification because a change in the amplification of one is accompanied by an equal change in the amplification of the other.

$$\psi = \overline{\Delta I}/I \quad , \qquad (11)$$

and

$$\overline{\Delta I} = \psi I \quad . \qquad (12)$$

A similar situation exists between I_c and $\overline{\Delta I}_c$ so that

$$\overline{\Delta I}_c = \xi I_c \quad . \qquad (13)$$

It was mentioned earlier that the r.m.s. fluctuations represented by $\overline{\Delta I}$ and $\overline{\Delta I}_c$ are not indepdnent of each other and are probably caused simultaneously by the same flame variations. It is reasonable to assume that the flame is in thermal and chemical equilibrium and homogeneous over the region being viewed and that these flame variations would cause the same degree of fluctuation in each intensity simultaneously, and so

$$\xi \cong \psi \quad . \tag{14}$$

Such an assumption was made for the theoretical treatments of this study. When Equations (9,10,12,13 and 14) are substituted into Equations (1) and (8), then

$$i = K_c W I \quad , \tag{15}$$

and

$$\overline{\Delta i}_T = \Big[K_d \left\{ i_d + K_c W [I_c R_d (W+W_m) + I] \right\} + (K_c W \psi)^2 [I_c R_d (W+W_m) + I]^2 \Big]^{1/2} \Delta f^{1/2} \quad . \tag{16}$$

Using Equations (15) and (16), the signal-to-noise ratio is then given by

$$i/\overline{\Delta i}_T = K_c W I / \Big[K_d \left\{ i_d + K_c W [I_c R_d (W+W_m) + I] \right\} + (K_c W \psi)^2 [I_c R_d (W+W_m) + I]^2 \Big]^{1/2} \Delta f^{1/2} \quad . \tag{17}$$

The derivation of the expression for the optimum slit width has been given by Winefordner and Vickers.[30] To find the optimum slit width Equation (17) is differentiated with respect to W, and when the derivative is set equal to zero the optimum value of W is found; that is, W_o. According to Winefordner and Vickers,[30] the differentiation step is easier if the square of the reciprocal of Equation (17) is differentiated with respect to W, and then W is optimized by setting the derivative equal to zero. Performing these steps, and substituting W_o for W to indicate that particular value of W found to be the optimum value, the following expression results

$$\begin{aligned}(2\Delta f\overline{\Delta I}_c{}^2R_d{}^2K_c{}^2)W_o{}^4 + (2\Delta f\overline{\Delta I}_c{}^2R_d{}^2W_mK_c{}^2)W_o{}^3 &+ \\ (2\Delta f\overline{\Delta I}_cR_d\,\psi K_c{}^2I)W_o{}^3 & \qquad (18) \\ -(K_d\Delta fI_cR_dW_mK_c)W_o - (K_d\Delta fK_cI)W_o - (2K_d\Delta fi_d) &= 0 \ .\end{aligned}$$

Equations (17) and (18) are the results of the mathematical derivation phase of this study. They are incorporated into a Fortran program (described in greater detail in Appendix 3) designed to calculate values for the signal-to-noise ratio as a function of integrated intensity values, I, and arbitrary slit width values, W, after evaluation of the various instrumental and flame compositional parameters appearing in the equations. The values for I are obtained from the results of other Fortran programs to be described later; these values for I are ultimately functions of the type of element and line, the sample concentration, the flame temperature, and flame type. Therefore, the calculated values of signal-to-noise ratio and of optimum slit width can be related to, and are functions of, those parameters.

It was necessary to derive suitable expressions for calculating the values of I as a function of element and line, sample concentration, flame temperature, and flame type. The general pattern for such derivations was available in the work of Vickers[24] in which he derived such an expression for I for the element sodium. This study extends those derivations to apply to the alkaline earths. For the case of the alkaline earths and the alkali metals, it is necessary to consider the metallic compound species that can be present in significant amounts in the flame gases.

The general approach to the derivation of an expression for I is to start with the molar concentration of the sample, C, and find the total partial pressure, P_T, in the flame gases of the aspirated metal in all of the forms in which it may be present (see Appendix 2 for relationships between C and P_T). Then the partial pressure, P_M, of only the atomic metal, M, and the number of metal atoms per cm^3 of flame gases, N, are calculated. From the N value, it is possible to calculate the integrated intensity and atomic absorption coefficient of metal M in the flame. By means of Fortran programs (see Appendix 2) designed for this study the intensity value, I, and the atomic absorption coefficient,

k^o, are calculated. The former is used in the calculations of signal-to-noise ratio for atomic emission flame spectrometry. The latter is not used specifically in this study but will be useful to a study, similar to this one, on atomic absorption flame spectrometry.

In Appendix 1, a discussion of the mathematical expressions and the Fortran program for the calculation of P_T values as a function of flame temperature, flame type, aspiration rate, and molar concentration of sample is given. The results of this program are printed out in tabular form where flame temperature and sample concentration are the two indexing dimensions of a table of P_T values. There is a separate page (and table) for each gas flow ratio of each different combination of fuel type and oxidant gas. These P_T values are independent of the type of metal in the sample solution; the coverage is broad, and both extrapolation and interpolation are easily possible in the use of the tables. The tables produced by this program should contain information of value for a variety of flame studies.

In Appendix 2, the mechanics and format of the Fortran program used to calculate values of the integrated intensity, I, as a function of element and line, P_T, flame temperature, and flame type are given. In order to obtain integrated intensities, various parameters must be known (see Appendix 2). To calculate the partial pressure, P_M, of the atomic metal species in the flame gases, several assumptions must be made. It must be decided which, of the possible compound and ion species of the metal, will be present in the flame gases in large enough quantities so as to subtract significantly from the concentration of the atomic metal species; that is, the only species capable of emitting light at the particular spectral line frequency being studied. The decision, as to whether or not a particular species is competing seriously with the metal species in concern, is based upon consideration of the concentration of the reactants, the size of the formation constant at the flame temperature, and the mechanics of the formation of a molecule of that species in a gaseous reaction. Values of dissociation constants over the range of flame temperatures, for a variety of species, are required in order to select properly those species to include in the equation for P_M. The JANAF tables[16] provided some of the dissociation constants; some are calculated by means of an equation given in Mavrodineanu and Boiteux;[20] and some of them are taken from the tables by Vickers.[23] Tables 1 through 5 list those values of the dissociation constants of the species assumed to be present in the flame for each of the five elements studied. Information as to the possible gaseous reactants present in the flame, and their partial pressures, is also required. This information is obtained from tables by

TABLE 1

DISSOCIATION CONSTANTS OF THE CHLORIDE, MONOXIDE, MONOHYDRIDE, AND MONOHYDROXIDE SPECIES, AND THE IONIZATION CONSTANTS, FOR SODIUM AT SEVERAL TEMPERATURES

Species	$NaCl$[a]	NaO[a]	NaH[a]	$NaOH$[a]	Na^+[b]
Temperature (K°)	(atm)	(atm)	(atm)	(atm)	(atm)
1800	$6.0 x 10^{-6}$	1.2	153.	$2.4 x 10^{-6}$	$1.0 x 10^{-13}$
2000	$9.1 x 10^{-5}$	1.8	137.	$4.1 x 10^{-5}$	$6.4 x 10^{-12}$
2200	$5.5 x 10^{-4}$	2.4	124.	$3.0 x 10^{-4}$	$1.7 x 10^{-10}$
2400	$3.2 x 10^{-3}$	3.1	115.	$2.0 x 10^{-3}$	$1.5 x 10^{-9}$
2600	$5.0 x 10^{-3}$	3.8	107.	$1.0 x 10^{-3}$	$5.0 x 10^{-9}$
2800	$4.2 x 10^{-2}$	4.6	102.	$3.1 x 10^{-2}$	$7.4 x 10^{-8}$
3000	$1.0 x 10^{-2}$	5.4	96.	$2.0 x 10^{-2}$	$4.0 x 10^{-7}$
3200	$1.4 x 10^{-1}$	6.2	91.	$2.5 x 10^{-1}$	$1.6 x 10^{-6}$

[a] Values taken from JANAF tables.[16]

[b] Values calculated by a standard equation as given in Mavrodineanu and Boiteux;[20] ionization potentials for calculations taken from Herzberg;[9] statistical weights of ion and atom taken from Mavrodineanu and Boiteux.[20]

TABLE 2

DISSOCIATION CONSTANTS OF THE CHLORIDE, MONOXIDE, MONOHYDRIDE, AND MONOHYDROXIDE SPECIES, AND THE IONIZATION CONSTANTS, FOR LITHIUM AT SEVERAL TEMPERATURES

Species	LiCl[a]	LiO[a]	LiH[a]	LiOH[a]	Li^+[b]
Temperature (K°)	(atm)	(atm)	(atm)	(atm)	(atm)
1800	1.3×10^{-8}	.060	12.	2.2×10^{-7}	4.1×10^{-14}
2000	1.4×10^{-7}	.12	15.	3.5×10^{-6}	1.9×10^{-12}
2200	9.2×10^{-7}	.22	17.	3.3×10^{-5}	3.6×10^{-11}
2400	4.5×10^{-6}	.36	20.	2.2×10^{-4}	4.7×10^{-10}
2600	1.7×10^{-5}	.55	22.	1.1×10^{-3}	4.4×10^{-9}
2800	5.4×10^{-5}	.79	24.	4.3×10^{-3}	2.9×10^{-8}
3000	1.5×10^{-4}	1.1	26.	1.4×10^{-2}	1.5×10^{-7}
3200	3.6×10^{-4}	1.4	28.	4.0×10^{-2}	6.4×10^{-7}

[a] Values taken from JANAF tables.[16]

[b] Values calculated by a standard equation as given in Mavrodineanu and Boiteux;[20] ionization potentials for calculations taken from Herzberg;[9] statistical weights of ion and atom taken from Mavrodineanu and Boiteux.[20]

TABLE 3

DISSOCIATION CONSTANTS OF THE CHLORIDE, MONOXIDE, MONOHYDRIDE SPECIES, AND THE IONIZATION CONSTANTS, FOR BARIUM AT SEVERAL TEMPERATURES

Species	$BaCl_2$[a]	BaO[b]	BaH[b]	Ba^+[c]
Temperature (K°)	(atm^2)	(atm)	(atm)	(atm)
1800	3.2x10^{-9}	1.2x10^{-8}	.046	5.0x10^{-13}
2000	1.2x10^{-7}	2.8x10^{-7}	.16	1.2x10^{-11}
2200	3.2x10^{-6}	3.5x10^{-6}	.46	3.8x10^{-10}
2400	5.7x10^{-5}	3.0x10^{-5}	1.1	4.6x10^{-9}
2600	7.1x10^{-4}	1.8x10^{-4}	2.3	3.9x10^{-8}
2800	7.9x10^{-3}	8.5x10^{-4}	4.4	2.5x10^{-7}
3000	7.7x10^{-2}	3.3x10^{-3}	7.7	1.2x10^{-6}
3200	5.6x10^{-1}	1.2x10^{-2}	12.	5.2x10^{-6}

[a] Values estimated by a method described by Vickers.[23]

[b] Values calculated by a standard equation as given in Mavrodineanu and Boiteux;[20] data for calculations taken from Vickers.[23]

[c] Values calculated by a standard equation as given in Mavrodineanu and Boiteux;[20] ionization potentials for calculations taken from Herzberg;[9] statistical weights of ion and atom taken from Mavrodineanu and Boiteux.[20]

TABLE 4

DISSOCIATION CONSTANTS OF THE CHLORIDE, MONOXIDE, MONOHYDRIDE SPECIES, AND THE IONIZATION CONSTANTS, FOR CALCIUM AT SEVERAL TEMPERATURES

Species	$CaCl_2$[a]	CaO[b]	CaH[b]	Ca^+[c]
Temperature (K°)	(atm^2)	(atm)	(atm)	(atm)
1800	6.3×10^{-9}	2.0×10^{-9}	.13	1.5×10^{-15}
2000	2.0×10^{-7}	5.4×10^{-8}	.43	1.0×10^{-13}
2200	6.0×10^{-6}	8.1×10^{-7}	1.1	3.3×10^{-12}
2400	1.3×10^{-4}	7.8×10^{-6}	2.6	5.9×10^{-11}
2600	2.0×10^{-3}	5.3×10^{-5}	5.3	7.0×10^{-10}
2800	2.2×10^{-2}	2.7×10^{-4}	9.6	5.9×10^{-9}
3000	2.0×10^{-1}	1.1×10^{-3}	16.	3.8×10^{-8}
3200	1.3	4.0×10^{-3}	26.	2.0×10^{-7}

[a] Values estimated by a method described by Vickers.[23]

[b] Values calculated by a standard equation as given in Mavrodineanu and Boiteux;[20] data for calculations taken from Vickers.[23]

[c] Values calculated by a standard equation as given in Mavrodineanu and Boiteux;[20] ionization potentials for calculations taken from Herzberg;[9] statistical weights of ion and atom taken from Mavrodineanu and Boiteux.[20]

TABLE 5

DISSOCIATION CONSTANTS OF THE CHLORIDE, MONOXIDE, MONOHYDRIDE SPECIES, AND THE IONIZATION CONSTANTS, FOR STRONTIUM AT SEVERAL TEMPERATURES

Species	$SrCl_2$[a]	SrO[b]	SrH[b]	Sr^+[c]
Temperature (K°)	(atm^2)	(atm)	(atm)	(atm)
1800	$1.1x10^{-9}$	$4.4x10^{-8}$	.12	$2.3x10^{-14}$
2000	$3.2x10^{-8}$	$8.6x10^{-7}$	.40	$1.2x10^{-12}$
2200	$7.2x10^{-7}$	$9.9x10^{-6}$	1.1	$3.0x10^{-11}$
2400	$1.3x10^{-5}$	$7.6x10^{-5}$	2.4	$4.5x10^{-10}$
2600	$1.8x10^{-4}$	$4.3x10^{-4}$	4.8	$4.6x10^{-9}$
2800	$2.0x10^{-3}$	$1.9x10^{-3}$	8.7	$3.4x10^{-8}$
3000	$2.0x10^{-2}$	$6.8x10^{-3}$	14.	$1.9x10^{-7}$
3200	$1.6x10^{-1}$	$2.1x10^{-2}$	23.	$9.0x10^{-7}$

[a] Values estimated by a method described by Vickers.[23]

[b] Values calculated by a standard equation as given in Mavordineanu and Boiteux;[20] data for calculations taken from Vickers.[23]

[c] Values calculated by a standard equation as given in Mavrodineanu and Boiteux;[20] ionization potentials for calculations taken from Herzberg;[9] statistical weights of ion and atom taken from Mavrodineanu and Boiteux.[20]

Hottel[11] and Zaer.[33] Table 6 lists the values for the partial pressures used in these calculations. In the case of barium, strontium and calcium, the monohydroxide is considered to be completely dissociated at flame temperatures. This is based on trends in the alkaline earth family and on statements by Lagerquist[12] and Sugden.[4,14,22] Because the program is intended to be also used with other elements in which the monohydroxide is of concern, the monohydroxide term is left in the program and, for these three elements, a suitably high value of the dissociation constant (100.) is used at each temperature. The total partial pressure of the electrons in the flame gases, P_e, is assumed to be due largely to the ionization of the flame gases. Gaydon[6] shows that the value for the electron pressure due only to ionization of flame gases, P_e', is approximately constant in all of the flames used in this study, and is $1. \times 10^{-9}$ atmospheres. In principle, the ionization of the metal will also contribute to the electron pressure, P_e. This increase in electron pressure is accounted for in the theoretical treatment given below. On the basis of the considerations mentioned above, the species that are assumed to be of interest under the flame conditions studied are: the monoxide, the monohydride, and the monohydroxide. In addition to these, the ionization constants for the first stage of ionization of the metal atom must be considered at the flame

TABLE 6

PARTIAL PRESSURES[a] OF THE ATOMIC SPECIES OF OXYGEN AND HYDROGEN, AND THE NEUTRAL HYDROXIDE SPECIES, IN THE FLAME GASES OF SEVERAL FLAMES

Species Flame type	O (atm)	H (atm)	OH (atm)
Stoichiometric hydrogen-oxygen[b] 2600 °K	3.6×10^{-3}	9.2×10^{-3}	3.3×10^{-2}
Fuel rich hydrogen-oxygen[b] H/O=4., 2600 °K	2.3×10^{-4}	2.7×10^{-2}	6.2×10^{-3}
Fuel rich hydrogen-oxygen[b] H/O=6., 2600 °K	1.2×10^{-4}	3.1×10^{-2}	3.6×10^{-3}
Stoichiometric hydrogen-air[b] 2200 °K	1.4×10^{-4}	4.9×10^{-4}	3.0×10^{-3}
Stoichiometric acetylene-oxygen[c] 2700 °K	6.3×10^{-3}	3.8×10^{-3}	4.6×10^{-2}
Fuel rich acetylene-oxygen[c] 2700 °K	3.6×10^{-3}	9.5×10^{-3}	9.1×10^{-2}

[a] Partial pressures given in units of atmospheres.

[b] Values taken from Hottel.[11]

[c] Values taken from Zaer.[33]

temperatures being used. The dissociation constant of the metal chloride is also included in the calculation because the metal is in that form when it is aspirated into the flame. The partial pressure of the atomic chlorine species is taken to be equal to P_T for the alkali metals (2 P_T for the alkaline earths) because the only source of chlorine is the metal chloride fed into the flame. Vickers[24] studied the effect of excess chlorine in the flame due to the presence of HCl in the sample solution and found that excess chlorine had negligible effect on the value of N unless the concentration of chloride is abnormally high. The dimetal oxide and the dihydroxide species are excluded from consideration because there is not a large enough concentration of the mono-form of these species present to form an appreciable amount of the di-forms of these species. The values of the ionization constants used (see Tables 1 through 5) were obtained by using an equation given in Mavrodineanu and Boiteux.[20]

Vickers[24,25] assumed that losses in the atomic concentration for sodium due to the formation of the monohydride and the monoxide are insignificant. The good agreement obtained between experimentally measured and theoretically calculated working curves, based on this assumption, indicated that it is a valid assumption. The dissociation constants for the lithium monoxide and the lithium monohydride indicated that the same assumption for lithium may not be as valid. Consequently, for convenience, the Fortran program for calculating N for the alkali metals also included these two species among the species considered. For the alkaline earths, the monohydride and monoxide must be considered. In Tables 7 and 8, values of N for both sodium and lithium, calculated by both assumptions, are given; that is, N values when the monohydride and monoxide species are included and N values when these species are ignored.

The general method of deriving an equation for P_M, in terms of P_T, dissociation and ionization constants, and partial pressures of flame gas products, is the same as that used by Vickers.[24] The expressions for the various equilibrium constants, each containing P_M, are combined algebraically and solved for P_M in terms of parameters whose values are known. In this case, the final expression is not simple to solve, and so the use of a Fortran program and a successive approximation technique is the most convenient way to obtain values of P_M from the equation derived here.

For the alkaline earth metals, the derivation proceeds as follows: M represents any of the alkaline earth metals; K_1, K_2, K_3, K_4 are the dissociation constants of the metal chloride, the metal monoxide, the metal monohydride, and the metal monohydroxide respectively; P_O, P_H, P_{OH} are the partial

TABLE 7

N^a VALUES FOR SODIUM IN THREE FLAMES CALCULATED WITH, AND WITHOUT CONSIDERATION OF THE MONOXIDE AND MONOHYDRIDE SPECIES

Flame type	Stoichiometric hydrogen-oxygen		Fuel rich hydrogen-oxygen		Stoichiometric acetylene-oxygen	
Method of calculation	With[b]	Without[c]	With[b]	Without[c]	With[b]	Without[c]
Temperature (K°)	(atoms cm^{-3})		(atoms cm^{-3})		(atoms cm^{-3})	
1800	3.0×10^{8}	3.0×10^{8}	1.7×10^{9}	1.7×10^{9}	2.1×10^{8}	2.1×10^{8}
2000	4.7×10^{9}	6.9×10^{10}	2.5×10^{10}	3.4×10^{11}	3.4×10^{9}	5.0×10^{10}
2200	3.1×10^{10}	1.5×10^{12}	1.5×10^{11}	2.8×10^{12}	2.2×10^{10}	1.2×10^{12}
2400	1.9×10^{11}	2.8×10^{12}	7.3×10^{11}	3.2×10^{12}	1.3×10^{11}	2.8×10^{12}
2600	8.6×10^{10}	2.5×10^{12}	3.9×10^{11}	2.6×10^{12}	5.9×10^{10}	2.5×10^{12}
2800	1.1×10^{12}	2.2×10^{12}	1.7×10^{12}	2.2×10^{12}	8.8×10^{11}	2.2×10^{12}
3000	6.1×10^{11}	1.3×10^{12}	1.1×10^{12}	1.3×10^{12}	5.3×10^{11}	1.3×10^{12}
3200	6.3×10^{11}	6.7×10^{11}	6.7×10^{11}	6.7×10^{11}	6.3×10^{11}	6.7×10^{11}

[a] Number of atoms per cm^3 of flame gases when the P_T value is $1. \times 10^{-6}$.

[b] N value calculated by an equation which includes consideration of the monohydride and monoxide species.

[c] N value calculated by an equation which does not consider the monohydride and monoxide species.

TABLE 8

N[a] VALUES FOR LITHIUM IN THREE FLAMES CALCULATED WITH, AND WITHOUT, CONSIDERATION OF THE MONOXIDE AND MONOHYDRIDE SPECIES

Flame type	Stoichiometric hydrogen-oxygen		Fuel rich hydrogen-oxygen		Stoichiometric acetylene-oxygen	
Method of calculation	With[b]	Without[c]	With[b]	Without[c]	With[b]	Without[c]
Temperature (K°)	(atoms cm^{-3})		(atoms cm^{-3})		(atoms cm^{-3})	
1800	2.7×10^{7}	2.7×10^{7}	1.5×10^{8}	1.5×10^{8}	2.1×10^{7}	2.1×10^{7}
2000	3.7×10^{8}	3.8×10^{9}	2.0×10^{9}	2.0×10^{10}	2.7×10^{8}	2.7×10^{9}
2200	3.4×10^{9}	2.0×10^{11}	1.8×10^{10}	6.9×10^{11}	2.5×10^{9}	1.5×10^{11}
2400	2.1×10^{10}	1.8×10^{12}	1.0×10^{11}	2.3×10^{12}	1.4×10^{10}	1.6×10^{12}
2600	9.5×10^{10}	2.4×10^{12}	4.1×10^{11}	2.5×10^{12}	6.5×10^{10}	2.4×10^{12}
2800	2.8×10^{11}	2.2×10^{12}	9.7×10^{11}	2.2×10^{12}	2.2×10^{11}	2.2×10^{12}
3000	5.8×10^{11}	1.6×10^{12}	1.2×10^{12}	1.6×10^{12}	5.0×10^{11}	1.6×10^{12}
3200	7.0×10^{11}	1.0×10^{12}	9.5×10^{11}	1.0×10^{12}	6.0×10^{11}	1.0×10^{12}

[a] Number of atoms per cm^3 of flame gases when the P_T value is $1.\times10^{-6}$.

[b] N value calculated by an equation which includes consideration of the monohydride and monoxide species.

[c] N value calculated by an equation which does not consider the monohydride and monoxide species.

pressures in the flame gases of the neutral species oxygen (O), hydrogen (H), and hydroxide (OH) respectively; K_5 is the first stage ionization constant of the metal; P_e' is the partial pressure of electrons due to ionization of flame gases (that is, with no sample present), and P_e is the partial pressure of electrons when those electrons from the ionization of the metal are included (that is, with sample present). It is assumed that the partial pressure of neutral chlorine (Cl) is twice the value of P_T because the aspirated metal chloride is the only source of either metal or chloride, and there is complete dissociation of the metal chloride. Therefore

$$P_{MCl_2} = P_M(2P_T)^2/K_1 \quad , \qquad (19)$$

$$P_{MO} = P_M P_O/K_2 \quad , \qquad (20)$$

$$P_{MH} = P_M P_H/K_3 \quad , \qquad (21)$$

$$P_{MOH} = P_M P_{OH}/K_4 \quad , \qquad (22)$$

$$K_5 = P_{M^+} P_e/P_M \quad . \qquad (23)$$

However, because the number of electrons added to the electron pressure by ionization of the metal is simply equal to P_{M^+} then

$$P_e = P_e' + P_{M^+} \qquad (24)$$

and Equation (23) becomes

$$K_5 = P_{M^+}(P_e' + P_{M^+})/P_M \quad . \tag{25}$$

By collecting terms in Equation (25) and arranging in the form of the quadratic equation where P_{M^+} is the variable, then

$$(P_{M^+})^2 + P_e'P_{M^+} - K_5P_M = 0 \quad . \tag{26}$$

The solution of Equation (26) is

$$P_{M^+} = -P_e' + [(P_e')^2 + 4K_5P_M]^{1/2}/2 \quad . \tag{27}$$

The total partial pressure, P_T, is equal to the sum of all of the partial pressures of the metal species, and so

$$P_T = P_M + P_{MCl_2} + P_{MO} + P_{MH} + P_{MOH} + P_{M^+} \quad . \tag{28}$$

Substituting Equations (19,20,21,22,27) into Equation (28) gives

$$\begin{aligned} P_T + P_M + [P_M(2P_T)^2/K_1] + (P_MP_O/K_2) + (P_MP_H/K_3) + \\ (P_MP_{OH}/K_4) + (-P_e' + [(P_e')^2 + 4K_5P_M]^{1/2}/2) \quad , \end{aligned} \tag{29}$$

and clearing Equation (29) of fractions and rearranging gives

$$\begin{aligned} 2(K_1K_2K_3K_4 + 4\ K_2K_3K_4P_T^{\ 2} + K_1K_3K_4P_O + K_1K_2K_4P_H + \\ K_1K_2K_3P_{OH})P_M + K_1K_2K_3K_4[(P_e')^2 + 4\ K_5P_M]^{1/2} - \\ K_1K_2K_3K_4(P_e' + 2\ P_T) = 0 \quad . \end{aligned} \tag{30}$$

The value of P_M in this expression is solved by successive approximations using the Fortran program described in

Appendix 2. A similar derivation for alkali metals differs only by the assumption below

$$P_{Cl} \cong P_T \quad . \tag{31}$$

Therefore the expression for the alkali metals which corresponds to Equation (30) is

$$2(K_1K_2K_3K_4 + K_2K_3K_4P_T + K_1K_3K_4P_O + K_1K_2K_4P_H + K_1K_2K_3P_{OH})P_M + K_1K_2K_3K_4[(P_e')^2 + 4\ K_5P_M]^{1/2} - K_1K_2K_3K_4(P_e' + 2\ P_T) = 0 \quad . \tag{32}$$

After values of P_M are calculated, values of N can be calculated from the P_M value by means of the Fortran program. The values of N are obtained from P_M simply by use of the ideal gas law equation. The partial pressure of the metal species is so low that the ideal gas law is a good assumption, and so

$$N = P_M/kT \quad , \tag{33}$$

where N is the atoms per cm^3, P_M is the partial pressure of the atomic species in atmospheres, k is the Boltzmann constant in cm^3 atmospheres °K^{-1}, and T is the flame temperature in degrees Kelvin.

The relationship of intensity of emitted light to number of atoms per cm^3 is discussed by Winefordner and coworkers.[30,32] Two expressions are given relating I and N. The symbols in these expressions are defined as: h is

Planck's constant in erg sec; ν_o is the frequency of maximum intensity of the spectral line in sec^{-1}; A_t is the transition probability in sec^{-1}; L is the average diameter or thickness of the flame region being viewed; g_u is the statistical weight of the upper state involved in the transition; k is the Boltzmann constant in units consistent with E_u and T; T is the absolute temperature of the flame gases; E_u is the excitation energy and $E_u = h\nu_o$ because the energy of the lower state is zero for the resonance line; c is the speed of light in cm sec^{-1}; $\Delta\nu_D$ is the Doppler half width of the spectral line in sec^{-1}; "a" is the ratio of damping broadening to Doppler broadening[10] times $\sqrt{\ln 2}$, no units, indicating the broadening of the spectral line due to classical broadening factors including the Doppler broadening; B(T) is the partition function over all states

$$I = [NLh\nu_o A_t g_u / 10^{-7}\, 4\pi\, B(T)]\ \exp(-E_u/hT) \quad , \qquad (34)$$

which is valid for values of N that are smaller than the so-called "intersection point" value of N,[32] and

$$I = (h\nu_o^2/10^7 c)[\Delta\nu_D\ g_u a N A_t L/\pi\sqrt{\ln 2}\, B(T)]^{1/2}$$
$$\exp(-E_u/kT) \quad , \qquad (35)$$

which is valid at values of N larger than the "intersection point" N value. Equations (34) and (35) are both required because at higher concentrations self-absorption of emitted light results in I being proportional to the square root of N, whereas at lower concentrations I is directly proportional to N. The "intersection point" value of N is that value of N above which self absorption is significant, and so I is given by Equation (35), and below which I is given by Equation (34). In the Fortran program in which I values are calculated from N values, a test is run on each N value to see if it is greater or less than the "intersection point" value in order that the correct equation is used to calculate the value of I. The "intersection point" value is calculated by the equation given by Winefordner, Vickers, and Remington[32]

$$N_i = 60[a\Delta\nu_D B(T)/A_t L\lambda_o^2 g_u] \quad . \tag{36}$$

The terms used are the same as those defined for Equations (34) and (35) except that λ_o is the wavelength of the peak of the spectral line. If $\Delta\nu_D$ is substituted[32] for in terms of atomic weight and temperature, then

$$N_i = 7.15 \times 10^{-7}[16\pi a\,\nu_o T^{1/2} B(T)/M_a^{1/2} \sqrt{\ln 2}\, g_u A_t L\lambda_o^2] \quad . \tag{37}$$

Equation (37) shows that the "intersection point" value of N is dependent on the flame temperature. Therefore the "intersection point" N values, used in the program for determining whether the N being considered is higher or lower than the "intersection point" N, are calculated by hand and are fed into the program as a set of data subscripted with the same symbol as the temperature data.

The calculation of k° values from N values is performed in the program by use of an altered form of the equation used by Winefordner and Vickers,[29] namely,

$$k^\circ = [2\sqrt{\ln 2}\,\lambda_o{}^2 g_u A_t\,\delta\,M_a{}^{1/2}/7.15\times10^{-7}\,\nu_o\sqrt{\pi}\,8\pi B(T)]NT^{-1/2}, \tag{38}$$

where δ is a factor which accounts for broadening factors other than Doppler broadening. The form in which the values of N, I, and k° are printed out by the program is given in Appendix 2.

IV. EXPERIMENTAL MEASUREMENTS

A. Measurement of Parameter Values

Measurements were made of the voltages between the cathode of the photomultiplier tube and the anode, as well as the voltage between the cathode and ground, for each sensitivity setting of the DU power supply unit connected to the DU. Different sensitivity settings resulted in different voltages across the photomultiplier tube. The circuit diagram in the instrument manual of the DU indicated that the signal from the photomultiplier tube was taken off of the final dynode. The anode of the tube was maintained at a more positive potential than the final dynode and was also more positive than the instrument ground potential. It was not convenient to measure the voltage between the cathode of the tube and the final dynode of the tube because these measurements were made with the phototube out of the instrument. It was assumed that the effective voltage applied to the photomultiplier tube by the DU was that applied between the cathode of the tube and the instrument ground. Measured voltages between the cathode and ground, and between the cathode and the anode for each sensitivity setting of the DU power supply unit are given in Table 9.

TABLE 9

MEASURED VOLTAGE BETWEEN THE CATHODE AND GROUND AND CATHODE AND ANODE OF THE PHOTOMULTIPLIER ON THE BECKMAN DU SPECTROPHOTOMETER AT SEVERAL SENSITIVITY SETTINGS

Sensitivity Setting[a]	Potential between cathode[b] and instrument ground (volts)	Potential between cathode and anode[c] (volts)
Full	640.	720.
9	535.	625.
8	455.	538.
7	395.	480.
6	340.	422.
5	295.	372.
4	250.	330.
3	210.	290.
2	175.	255.
1	150.	232.

[a] Sensitivity dial settings on the DU power supply unit.

[b] Cathode post of the RCA IP28 photomultiplier tube socket (the photomultiplier tube was not in the instrument during the measurement).

[c] Anode post of the RCA IP28 photomultiplier tube socket.

In the program used for calculating signal-to-noise ratio and optimum slit width values, the anodic dark current, i_d, the gain factor, M, and the amperes per watt factor, γ, are treated as constant values. No allowance was made for variation of their values to correspond to the different voltages of different sensitivity settings. Most of the signal-to-noise ratio measurements made on the DU were obtained on one of three sensitivity settings: Full, 9, or 8. Therefore, the voltage applied to the photomultiplier tube was taken as 530 ± 10 volts which was an average value of these three settings. The dark current was measured at 522 volts, and M and γ were measured at 535 volts.

1. Photoanodic dark current values, i_d

The photoanodic dark current of the 1P28 photomultiplier tube used in this study was measured using the Jarrell-Ash monochromator and the Jarrell-Ash dc electrometer-readout system. With this instrumental arrangement, the signal was read directly in amperes. The signal produced when a certain voltage was applied across the photomultiplier tube, with the slit closed, was considered to be the photoanodic dark current flowing through that tube under that voltage. In the Jarrell-Ash system, the signal was taken from the anode of the photomultiplier tube rather than from the final dynode as in the Beckman DU. The voltage between the cathode and ground on the DU corresponded to the voltage between the cathode and anode of the photomultiplier tube in the Jarrell-Ash. Measured values of i_d at various potentials applied across the photomultiplier tube are listed in Table 10.

2. Photosensitivity factor values, γ

The values of in amperes per watt were measured using the same 1P28 photomultiplier tube that was used in the Beckman DU and the Jarrell-Ash instrumental system. The filament of a standard light source was focused by a bi-convex lens to give a spot of light on the slit opening of the monochromator which completely illuminated the slit. Care was taken to see that the aperture of the lens outside the slit was less than the aperture of the collecting lens inside the instrument. Thus the inside lens was the one which determined the solid angle of light that was eventually focused on the grating of the monochromator. The resulting signal was read directly in amperes on the recorder. The slit area and internal optics of the monochromator were known and, consequently, Equation (1) could be solved for γ which was the only remaining unknown parameter. The values of γ were measured at the wavelengths of each of the spectral lines being studied; the voltage across the photomultiplier tube was the same for each wavelength setting, but the slit width was altered in each case to produce an accurately

TABLE 10

MEASURED[a] PHOTOANODIC DARK CURRENT VALUES AT SEVERAL VOLTAGES APPLIED[b] TO THE PHOTOMULTIPLIER TUBE

Tube voltage (volts)	Dark current (amperes)
630	1.6×10^{-10}
609	1.5×10^{-10}
522	1.0×10^{-10}
435	8.0×10^{-11}

[a] Measured on the dc electrometer readout system of the Jarrell-Ash instrumental arrangement used in this study.

[b] Voltage applied between the anode and cathode of the RCA IP28 photomultiplier tube by the dc power supply unit of the Jarrell-Ash instrumental arrangement used in this study.

measurable signal. Values of γ as measured for each wavelength setting are listed in Table 11.

3. Photomultiplier tube gain values, M

An attempt was made to measure the values of M, the total gain or magnification factor of the photomultiplier tube. The plan was to short out the dynodes of the photomultiplier tube, to replace them with resistors equal to the resistances between the dynodes, and to compare the signals obtained with the dynodes in the circuit and the signals obtained with the dynodes shorted out of the circuit. These efforts to measure M were not entirely satisfactory. The signals obtained with the dynodes shorted out were quite insensitive to variations in slit width and gave nearly constant values at each wavelength setting. A single approximated value of M, very close to the value obtained with the measurement technique described above, was used in the program for calculating the signal-to-noise ratios. This value, 10^5 (no units) obtained by measuring the particular photomultiplier tube used, was tenfold smaller than that used by Vickers[24] who estimated a value of M at 10^6 based on the manufacturer's claims for a good photomultiplier tube. The value of 10^5 for M, at this tube voltage, was also indicated by Lion.[19]

In this work, it was assumed that M and γ were not independent but were rather directly and simply related to

TABLE 11

MEASURED VALUES OF THE PHOTOSENSITIVITY FACTOR[a] AT SEVERAL WAVELENGTHS

Wavelength (Å)	Photosensitivity factor (amp. watt^{-1})
6708	1.5
5890	87.
5536	210.
4601	570.
4227	450.

[a] A voltage of 535 volts was being applied the cathode and anode of a RCA IP28 photomultiplier tube on the Jarrell-Ash instrumental arrangement used in this study.

each other. Therefore this pair of parameters were varied simultaneously by the same factor as that used on a single independent parameter.

4. Continuum intensity values, I_c

The measured values of the flame continuum intensity, I_c, in watts cm^{-2} $ster^{-1}$ $m\mu^{-1}$ were obtained by two different methods; approximate values for this parameter are also available from a graph by Gilbert.[7] The first method, and the method whose values of I_c were eventually used in the theoretical treatment of this study, involved measurement of the signal of the blank, i_w, run with each measurement of a sample signal, i_s. For each signal measurement, a base line (shutter closed) was established, a blank (distilled water being aspirated into the flame) was measured, and the sample (sample solution being aspirated into the flame) was measured. There is also available, in the data printed out by the programs described in Appendix 1 and 2, values of the sample intensity, I, in watts cm^{-2} $ster^{-1}$ for that particular sample concentration, aspiration rate, flame condition, and spectral line. If it is assumed that these theoretical values of I are valid, then the ratio of I (intensity of the sample in watts cm^{-2} $ster^{-1}$) to I_{cw} (intensity of the flame continuum in watts cm^{-2} $ster^{-1}$-- assuming that distilled water adds nothing to the intensity of the signal of the blank but also serves to make the temperature and shape of the flame the same for the blank as it is for the sample) is equal to the ratio of the sample signal to the water signal. This proportion is expressed in the equation

$$I/I_{cw} = i_s/i_w \tag{39}$$

The values of the ratio on the right side of Equation (39) can be measured on the recorder chart paper. Using these ratios, and the theoretical values of I, the absolute values of I_{cw} can be calculated by Equation (39). The units of the continuum term, I_c, to be used in Equation (17) are watts cm^{-2} $ster^{-1}$ $m\mu^{-1}$. Values of I_{cw} can be converted to I_c values by dividing I_{cw} by the spectral slit width, s. The value of s can be obtained from Equation (7) ($s = R_dW$ if $W \gg W_m$). Values of R_d are available in the manufacturer's literature for the monochromator. The values obtained by this method of measuring I_c are only as accurate as the theoretically obtained values of I.

The second method of measuring I_c consisted of using a standard light source on the Jarrell-Ash monochromator--Sargent recorder. The signal in amperes, produced when the standard light source was focused on the entrance slit of the monochromator, was measured. Also the signal produced when distilled water was aspirated into a flame placed in the same optical location of the standard light source was measured. The ratio of these two signals is the same as the ratio of signals on the right side of Equation (39), and so these signal ratio values, along with the values of I taken from the calibration table for the standard source, make it possible to use Equation (39) to calculate values of I_{cw}. The values of I_{cw} thus obtained can also be converted to corresponding values of I_c by dividing them by the spectral slit width (s) if $W \gg W_m$. In the case of the Jarrell-Ash monochromator, which is a grating instrument, a single value of R_d is valid for all wavelengths (as compared to the DU which is a prism instrument). However, with the Jarrell-Ash measurements, it was necessary to use a different slit width with the standard source than was used with the flame because of the large difference in intensity of the two. This made it necessary to correct the flame intensity reading by a factor that was the square of the ratio of the two slit widths. The most likely source of error in this method of measuring I_c was in the mechanical difficulties of obtaining the same flame conditions and optics, for the I_c measurement, as was used on the signal measurement with which the theoretical calculations using I_c are supposed to agree. The flame used for the I_c measurement on the Jarrell-Ash might not be in exactly the same location of the entrance optics as the standard source was. The height of the entrance slit of the monochromator above the tip of the burner could be different between the Jarrell-Ash, where I_c was measured, and the DU where the signal-to-noise ratio was measured. Therefore the monochromator would view a different region of the flame which could have a different temperature and different continuum intensity. The same burner was used on both instruments, but it was mounted differently for each. Therefore some differences of gas flow rate and aspiration rate between the two different mountings of the burner could occur. It is likely that the voltages applied to the photomultiplier tube by the two systems differed although this will be shown not to be a source of significant error. Most of the errors dealing with variations of optics and flame conditions were not present in the measurements made on the DU in the first method because the same flame, aspiration rate, gas flow rate, and monochromator setting that was used for the I_c measurement (distilled water aspirated into the flame) was used only a fraction of a minute later for the signal measurement (sample solution aspirated into the flame). However in the first method, it was necessary to rely on theoretically calculated intensity values. Consequently there was some doubt as to the validity of either method for use in measuring I_c. It was decided, on the basis of agreement between experimentally and theoretically produced curves of signal-to-noise ratio versus slit width, that the I_c values measured on the DU gave slightly better agreement, and so these were the ones that were used in the theoretical treatment of this study. In Table 12 the values of I_c measured on the DU and on the Jarrell-Ash, are given as well as values read from the graph of Gilbert,[7] for each flame type and each wavelength studied.

5. Flame flicker parameter values, ψ

The flame flicker noise was assumed to be a constant fraction, ψ , of the emitted intensity. Most of the other sources of noise (shot effect, Johnson noise, etc.) arose in the instrument and were not dependent on flame conditions. Consequently they did not increase with intensity as the flame flicker noise did. Therefore at high sample concentrations, and high intensity values, the flame flicker noise should be the predominant noise, and the others should make a negligible contribution to the total r.m.s. noise, $\overline{\Delta i}_T$. The continuum intensity did not increase with the intensity of the atomic line, and so the fluctuation in the continuum intensity due to flame flicker should also not increase with emitted intensity from the sample atoms. Therefore, at a high sample intensity, the flicker in the flame continuum should also make a negligible contribution to $\overline{\Delta i}_T$ even though such noise has its origin in the flame

TABLE 12

FLAME CONTINUUM INTENSITY VALUES,[a] OBTAINED BY TWO METHODS OF MEASUREMENT AND ONE LITERATURE SOURCE, AT FIVE WAVELENGTHS IN THREE FLAME TYPES

Flame type	Stoichiometric hydrogen-oxygen			Fuel rich[b] hydrogen-oxygen		Stoichiometric acetylene-oxygen		
Source of value	I[c]	II[d]	III[e]	I[c]	II[d]	I[c]	II[d]	III[e]
	(watt $cm^{-2}ster^{-1}m\mu^{-1}$) ($X10^{-7}$)			(watt $cm^{-2}ster^{-1}m\mu^{-1}$) ($X10^{-7}$)		(watt $cm^{-2}ster^{-1}m\mu^{-1}$) ($X10^{-7}$)		
Wavelength of spectral line (Å)								
6708	.33	3.8	.10	1.1	7.5	95.	27.	.45
5890	.12	.67	.10	.029	1.4	.46	1.4	.70
5536	30.	.53	.08	47.	6.2	660.	.96	.75
4601	6.7	.16	.08	3.8	.20	53.	.51	1.7
4227	4.9	.086	.10	2.8	.13	130.	.49	3.2

[a] Flame continuum intensity values in watts $cm^{-2}ster^{-1}m\mu^{-1}$.

[b] Hydrogen-to-oxygen ratio is 4.

[c] Calculated by assigning intensity values to thermal emission signals measured on the Beckman DU and comparison with the signal measured for a blank aspirated into the flame.

[d] Calculated by using a standard light source on the Jarrell-Ash instrumental arrangement and comparison of that signal with the signal of a blank aspirated into the flame.

[e] Gilbert.[7]

conditions. When these assumptions are applied to Equation (17), those terms in which K_d or I_c appear will drop out leaving

$$i/\overline{\Delta i}_T = K_cWI/\Delta f^{1/2}K_cWI\,\psi = 1/\Delta f^{1/2}\psi \quad . \qquad (40)$$

If the signal-to-noise ratio at high I values is known, and if Δf is known, Equation (40) can be solved for the parameter ψ. In this study, four of the measured values of signal-to-noise ratio at different slit widths, for the most concentrated solutions of both barium and strontium were averaged for each type of flame. In Table 13, values of signal-to-noise ratio were averaged for each flame type and calculated values of ψ determined for each flame are given.

6. Frequency response band width values, Δf

According to Equation (17), the signal-to-noise ratio is inversely proportional to the square root of Δf. Errors in the value of Δf should cause an upward or downward displacement of the signal-to-noise ratio versus slit width curve but should not distort the shape of the curve. Therefore, in evaluating the agreement between experimental and theoretical signal-to-noise ratio versus slit width curves, more attention was given to agreement in the shape of the curves and less to the vertical alignment.

All of the noises considered in Equation (16) are white; that is, they are equally distributed at all

TABLE 13

MEASURED VALUES OF THE SIGNAL-TO-NOISE RATIO AT HIGH CONCENTRATIONS FOR THE CALCULATION OF FLAME FLICKER FACTOR VALUES

Flame type	I[b]	II[c]	III[d]
High concentration Signal-to-noise ratio Values considered	55.	70.	38.
	59.	95.	43.
	64.	78.	30.
	61.	89.	38.
	41.	56.	28.
	45.	61.	32.
	45.	95.	31.
	47.	75.	35.
Average signal-to-noise ratio value	52.	77.	34.
Calculated flame flicker factor	3.2×10^{-3}	2.2×10^{-3}	4.8×10^{-3}

[a] A Δf value of 36 cps was used for these calculations.

[b] Stoichiometric hydrogen-oxygen flame.

[c] Fuel rich hydrogen-oxygen flame.

[d] Stoichiometric acetylene-oxygen flame.

frequencies. The Beckman DU circuitry includes an RC filter network on the signal introduced into the input of the DU amplifier. This filter reduces the value of Δf and thus cuts out a considerable amount of the noise. The condenser of this filter was disconnected for the signal-to-noise ratio measurements of this study. The only filtering action left in operation was the time constant of the Heathkit recorder. If a noise of sufficiently high frequency, such that the recorder pen could not keep up with it, should try to come through with the signal, that frequency of noise would not be recorded. Consequently the value of Δf was limited by the time it took the pen to travel over that noise band distance on the chart (see Figure 1). The estimated average width of the noise band at mid-chart was 0.28 inches. The time required for the pen to travel full scale (10 inches) is one second. Therefore the value of Δf is 36 cps.

This method does not, however, account for the change in amplification with change in sensitivity setting on the DU power supply. If the input signal should fall low on the chart, the average noise signal will have a width less than the 0.28 inches which it would have had at the mid-chart location. Therefore the value of Δf for measurements in which the noise band width is less than 0.28 inches is greater than 36 cps. Conversely, an average noise signal falling high on the chart would be under a higher amplification factor and would establish a thicker noise band than 0.28 inches and would require a longer time to do so, and so a value lower than 36 cps would result. The computer program for calculating signal-to-noise ratio treated the parameter Δf as a constant. It did not allow for variation of the value of Δf with pen position, and so some single value of Δf had to be decided upon. The average mid-chart width of the noise band was chosen to establish that Δf value (36 cps) which was used in the theoretical treatment of this study.

To account for the variation in Δf with recorder pen position, the measured noise was multiplied by a factor to account for this variation and to normalize all noises to the middle of the recorder chart. Then theoretical and experimental values of signal-to-noise ratios should be directly comparable. The r.m.s. noise, as measured, was multiplied by a correction factor based on the decade of the chart paper in which the signal carrying the noise happened to fall. The measured r.m.s. noise was decreased for measurements in decades lower than the fifth decade and was increased for signals falling in decades above the fifth. The effect of the correction factor was to give all of the r.m.s. noise measurements that value which they would have had if they had all been measured in the fifth decade.

An attempt was made to verify the assumption that the limitation of pen speed constituted a filtering device operating in the instrumental arrangement and was therefore actually establishing the frequency response band width, Δf. A dc power supply and an audio frequency generator were both connected to the Heathkit recorder. The dc signal could be adjusted so as to place the pen in any decade of the chart paper. An independent ac noise signal was imposed on top of the dc signal. Both the energy and the frequency of the noise signal could be varied from zero upwards. With this arrangement, it was possible to determine Δf as a function of the fraction of full-scale recorder response. However, this instrumental arrangement also revealed that the pen speed of the recorder would readily pass harmonics of higher frequencies than the estimated 36 cps. Therefore, it was impossible to obtain an absolute value of Δf. As a result, little significance was attached to any vertical displacement of the theoretical signal-to-noise ratio versus slit width curve from the experimental curve. More significance was placed on the curve shape which was not affected by errors in the value of the parameter Δf.

7. Electrometer and photomultiplier tube noise values, $\overline{\Delta i}_e/\sqrt{\Delta f}$ and $\overline{\Delta i}_p$

With the shutter on the DU closed and the sensitivity set at various photomultiplier tube voltages, the total noise on the recorder (pen set at mid-chart) was due to the quadratic sum of the shot effect (and other noises originating in the photomultiplier tube) plus the electrometer noise (originating in that part of the circuitry following the photomultiplier tube)

$$\overline{\Delta i}_T = (\overline{\Delta i}_e{}^2 \Delta f + \overline{\Delta i}_p{}^2)^{1/2} \quad , \qquad (41)$$

where $\overline{\Delta i}_e\sqrt{\Delta f}$ is the electrometer noise and $\overline{\Delta i}_p$ is the phototube noise. An expression for the total noise that includes the electrometer noise would be an alteration of Equation (16) as follows:

$$\overline{\Delta i}_T = \Big[\Delta f \Big\{ K_d[i_d + K_c W \Big(I_c R_d (W+W_m) + I \Big)] + (K_c W \psi)^2 [I_c R_d (W+W_m) + I]^2 + \overline{\Delta i}_e{}^2 \Big\} \Big]^{1/2} \qquad (42)$$

If, with the same instrumental situation, the voltage across the photomultiplier tube is reduced to zero by turning the sensitivity setting to "off," the recorded noise will then be only the electrometer noise. Then by adjusting the DU sensitivity setting at "off," the value of $\overline{\Delta i}_p$ could be solved for using Equation (41). The electrometer noise signal, $\overline{\Delta i}_e\sqrt{\Delta f}$, was found to be negligible compared to $\overline{\Delta i}_p$ and so was eliminated from consideration in the derivation of Equation (17).

B. Methods of Obtaining and Evaluating Experimental Measurements of Signal-to-Noise Ratio

Three different sample concentrations differing by tenfold and ranging over a hundredfold were chosen for each of the five elements studied. However, the same series of concentrations was not used for all elements. Each element was studied on the DU instrumental arrangement in order to determine the hundredfold concentration range over which signals could be measured. The lowest concentration for most of the elements studied was somewhat above the limit of detectability. This instrumental arrangement had a lower sensitivity due to the blocked mirror, and so there was difficulty in covering the full hundredfold concentration range in some cases. The concentration ranges and spectral lines that were used are:

Barium	10 ppm to 1000 ppm	5536 Å
Calcium	0.1 ppm to 10 ppm	4227 Å
Lithium	10 ppm to 1000 ppm	6708 Å
Sodium	0.1 ppm to 10 ppm	5890 Å
Strontium	1.0 ppm to 100 ppm	4601 Å

All of the spectral lines studied, except sodium, were single, sharp, and isolated as required by the assumptions made in deriving Equation (17). In the case of the sodium doublet, 5890-5896 Å, the monochromator wavelength setting on the DU was maximized with respect to the signal, and the setting fell between the two lines. In this case, of course, the ξ factor described in Equation (1) does not have a value of unity. However, this error was ignored in the calculations because it was assumed that the error in the calculated signal-to-noise ratio introduced, was negligible compared to some of the experimental errors introduced into the measured signal-to-noise ratio. This difficulty did not arise during the use of the Jarrell-Ash monochromator which was capable of isolating the separate lines of the sodium doublet. In that oase, the 5890 Å line was measured because it is the stronger of the two.

Standard solutions of all metal salts as chlorides were prepared. As long as the metal salt was nearly completely dissociated in the flame, it made little difference which salt of the metal was used in preparing the sample.

Each of the three concentrations of each of the five elements was measured at a series of slit width values in each of three different flame types: stoichiometric hydrogen-oxygen ($H_2/O_2 = 2$), fuel rich hydrogen-oxygen ($H_2/O_2 = 4$), and stoichiometric acetylene-oxygen ($C_2H_2/O_2 = 2/5$).

The aspiration rate was measured prior to each series of recorder readings for each concentration of each element. The aspiration rate was measured by recording the time necessary to aspirate 4.00 ml of water. Three or four such measurements were averaged for each reported measurement of the aspiration rate.

The signal and noise measurements were made on the DU under the following instrumental conditions: the zero-suppress on the DU power supply was on the number 2 position; the sensitivity dial on the DU was in full clockwise position; the selection switch on the DU was set at 1; the zero-suppress on the external ammeter was set at midscale (500); the damping on the recorder was turned off; both the zero position dial and the calibration dial on the recorder was turned off; both the zero position dial and the calibration dial on the recorder were in full counterclockwise position; the mv range selection switch on the recorder was set at 10. The above settings were maintained throughout all of the signal and noise measurements on the DU. The three controls that were varied from reading to reading were the slit width, which was set at arbitrarily chosen values; the dark current dial on the DU, which set the base line at zero on the chart; the sensitivity setting on the DU power supply, which was adjusted to keep the signal on the chart paper throughout the range of slit widths and concentrations.

To establish the recorder base line, the following procedure was observed: the shutter was closed; the blank signal with distilled water only being aspirated into the flame was measured; the signal (and noise) was measured by allowing the sample solution to aspirate approximately two full minutes (an inch on the chart paper). In Figure 1 a typical chart reading of the base line, blank, and signal is given.

The translation of the recorded signals into values of the signal-to-noise ratio requires some explanation. The signal value was taken to be the distance in inches between a line, parallel to the base line and running through the center of the noise band of the blank signal, and a similar line running through the center of the noise band of the sample signal. The peak-to-peak noise was taken to be the width in inches of that solid black portion of the noise band of the sample signal. This peak-to-peak width was then divided by two in order to consider that half of the noise band lying above the signal line and also divided by the square root of two to convert it to r.m.s. noise (see Figure 1).

The boundaries of the solid black portion of the noise band were obtained by use of considerable judgment on the part of the operator. In fact, this step introduced sufficient error into the value of the measured signal-to-noise ratio to partially nullify any argument that might be based on the exact agreement between theoretically determined and measured signal-to-noise versus slit width curves. The estimation of the noise boundaries is necessary because of

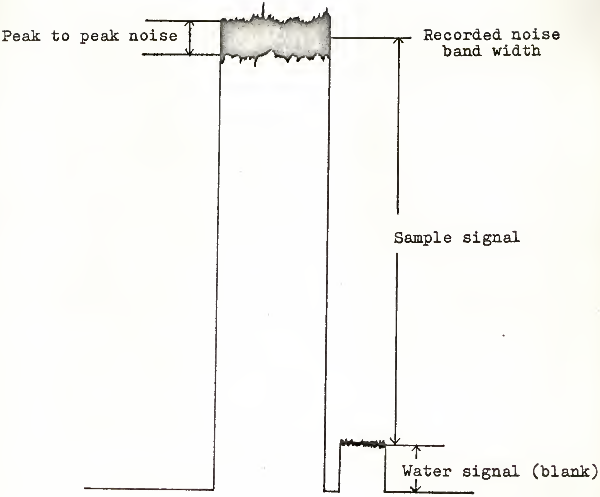

Fig. 1.-Typical chart readout, with interpretation, for measurement of signal and noise.

the following factors: (a) there are, at some times, spurious peaks in the noise pattern reaching well beyond the solid portion; (b) also, at some times, there was an apparently very low frequency noise wave pattern which lifted and lowered the whole solid portion; (c) most of the time, the boundary of the solid band was not a sharp line but irregularly saw-toothed. The total area between the signal line as the base boundary and the pen mark (or noise line) as the upper boundary represents the r.m.s. noise energy. It was assumed that the solid part of the noise band represented the great majority of this area because the solid portion was formed by many peaks overlapping each other due to the slow chart speed. Consequently, the spurious peaks above this line represented an insignificant percentage of the total area to warrant inclusion of their area in the measurement. The low frequency wave motion affecting the whole noise band resembled, and was assumed to be due to, the pattern shown when certain harmonics of higher frequency noises are being passed, by the pen speed filter. In such cases, it was assumed that the noise energy that fell within the 36 cps band width range was still represented by the solid black portion (even though it was undulating) and so the width of the solid black part of the band was reported as the peak-to-peak noise. The lack of a sharp boundary for the solid band resulted in a fixed error in reading the width of this band in inches.

The width of the solid black noise band was measured visually with the aid of a micrometer which read to the thousandth of an inch. The micrometer was laid on the chart paper and the reader's eye passed back and forth from the edge of one micrometer jaw to the edge of the other jaw until it was felt that parallax had been minimized at both jaw surfaces. The width of the noise band on each signal was measured at several points with the micrometer until a satisfactory agreement among the measurements had been reached.

Attempts were made to measure the noise by other methods than that described above. An attempt was made to measure the electrical energy of the noise signal with a r.m.s. frequency meter, but it was not possible to obtain a meter that would measure energy down to near dc frequencies. An attempt was also made to measure the total area between the signal boundary and the upper noise line boundary by using fast chart speed (four inches per minute) and a planimeter. It was found that the total area was too small, and the shape too irregular, to obtain sufficient accuracy to make such tedious work worthwhile. The r.m.s. noise, measured as described above, was multiplied by the correction factor to compensate for variations due to the decade of the chart paper in which the signal fell (described in the section on Δf) and then used as the denominator of the signal-to-noise ratio.

It was estimated that an error of 0.02 inches was introduced into the peak-to-peak noise measurement of the noise band because of the lack of a sharp boundary for this portion of the band. The percent of error that this fixed reading error introduced was calculated for each reading, and the corresponding percent error that it caused in the value of the signal-to-noise ratio was calcuated. These percentage error values are listed along with the measured signal-to-noise ratio values in Tables 14 through 28, and the effect of the error is also indicated in the graphs of signal-to-noise ratio versus slit width that are reproduced in this work.

C. Comparison of the Theoretical and Experimental Plots of Signal-to-Noise Ratio Versus Slit Width

The purpose of this study was to determine the size of the optimum slit width in various situations as well as the sensitivity of the signal-to-noise ratio to the slit width, that is, the shape of the maximum of the signal-to-noise ratio versus slit width curve. It was further intended to demonstrate the validity of Equation (17), and therefore the validity of further conclusions drawn concerning the influence of individual parameters, by showing agreement in both shape and magnitude between the calculated and measured plots of signal-to-noise ratio versus slit width. The

TABLE 14

ALCULATED AND MEASURED SIGNAL-TO-NOISE RATIOS FOR THREE CONCENTRATIONS OF BARIUM IN A STOICHIOMETRIC HYDROGEN-OXYGEN FLAME[a]

Concentration (ppm)	10.		100.		1000.	
Study Slit Width (µ)	Calculated	Measured	Calculated	Measured	Calculated	Measured
30.	30.	-	47.	14. ± 2.	51.	46. ± 4.
50.	28.	-	47.	14. ± 2.	50.	46. ± 2.
70.	26.	4. ± .5	46.	24. ± 2.	50.	43. ± 3.
90.	24.	6. ± .6	46.	27. ± 2.	50.	52. ± 3.
110.	23.	8. ± .8	44.	33. ± 2.	50.	55. ± 3.
400.	14.	7. ± .4	35.	53. ± 6.	45.	59. ± 7.
800.	10.	8. ± .6	29.	47. ± 6.	42.	64. ± 5.
1000.	8.0	7. ± .4	26.	39. ± 3.	39.	61. ± 6.
Optimum slit width (µ)[b]	15.		15.		15.	

[a] Estimated flame temperature[28] 2665. °K; hydrogen flow rate 5,000. cm^3min^{-1}; oxygen flow rate 2,500. cm^3min^{-1}; sample aspiration rate 1.72 cm^3min^{-1}; wavelength 5536 Å; atomization efficiency factor, ϵ,[27] estimated at 0.5.

[b] Calculated optimum slit width.

TABLE 15

CALCULATED AND MEASURED SIGNAL-TO-NOISE RATIOS FOR THREE CONCENTRATIONS OF BARIUM IN A FUEL RICH HYDROGEN-OXYGEN FLAME[a]

Concentration (ppm)	10.		100.		1000.	
Study Slit Width (μ)	Calculated	Measured	Calculated	Measured	Calculated	Measured
30.	56.	10. ± 1.	71.	34. ± 2.	74.	53. ± 4.
50.	53.	16. ± 2.	71.	41. ± 3.	74.	62. ± 6.
70.	50.	16. ± 1.	70.	42. ± 2.	73.	65. ± 5.
90.	47.	21. ± 2.	69.	62. ± 7.	73.	73. ± 9.
110.	45.	26. ± 3.	68.	52. ± 5.	73.	70. ± 7.
400.	25.	19. ± 3.	57.	68. ± 9.	69.	95. ± 19.
800.	20.	16. ± 2.	49.	71. ± 12.	65.	78. ± 8.
1000.	14.	13. ± 1.	42.	50. ± 5.	61.	89. ± 15.
Optimum Slit Width (μ)[b]	20.		20.		20.	

[a] Estimated flame temperature[28] 2645. °K; hydrogen flow rate 10,000. $cm^3 min^{-1}$; oxygen flow rate 2,500. $cm^3 min^{-1}$; sample aspiration rate 1.56 $cm^3 min^{-1}$; wavelength 5536 Å; atomization efficiency factor, ϵ ,[27] estimated at 0.5.

[b] Calculated optimum slit width.

TABLE 16

CALCULATED AND MEASURED SIGNAL-TO-NOISE RATIOS FOR THREE CONCENTRATIONS OF BARIUM IN A STOICHIOMETRIC ACETYLENE-OXYGEN FLAME[a]

Concentration (ppm)	10.		100.		1000.	
Study Slit Width (µ)	Calculated	Measured	Calculated	Measured	Calculated	Measured
30.	9.3	-	26.	8.5 ± 1.2	32.	37. ± 4.
50.	8.2	-	24.	8.5 ± 0.5	31.	38. ± 2.
70.	7.1	-	23.	6.2 ± 0.3	29.	43. ± 4.
90.	6.5	-	22.	5.8 ± 0.2	29.	30. ± 2.
110.	5.9	-	20.	6.3 ± 0.2	28.	38. ± 2.
400.	2.7	-	12.	3.7 ± 0.2	21.	22. ± 1.
800.	1.8	-	18.	2.5 ± 0.1	17.	24. ± 1.
1000.	1.3	-	7.0	2.5 ± 0.1	15.	29. ± 3.
Optimum Slit Width (µ)[b]	10.		10.		10.	

[a] Estimated flame temperature[28] 2937. °K; acetylene flow rate 1,400. cm^3min^{-1}; oxygen flow rate 3,500. cm^3min^{-1}; sample aspiration rate 1.81 cm^3min^{-1}; wavelength 5536 Å; atomization efficiency factor, ϵ ,[27] estimated at 0.5.

[b] Calculated optimum slit width.

TABLE 17

CALCULATED AND MEASURED SIGNAL-TO-NOISE RATIOS FOR THREE CONCENTRATIONS OF CALCIUM IN A STOICHIOMETRIC HYDROGEN-OXYGEN FLAME[a]

Concentration (ppm)	0.1		1.0		10.	
Study Slit Width (μ)	Calculated	Measured	Calculated	Measured	Calculated	Measured
30.	1.0	-	7.3	-	24.	15. ± 2.
50.	.92	-	6.8	-	24.	16. ± 2.
70.	.83	-	6.4	4.2 ± 0.6	23.	22. ± 2.
90.	.71	-	5.9	5.6 ± 1.	22.	22. ± 2.
110.	.65	-	5.2	5.2 ± 0.5	21.	22. ± 1.
400.	.24	-	2.1	3.8 ± 0.5	12.	15. ± 1.
800.	.14	-	1.0	2.4 ± 0.3	9.0	14. ± 0.2
1000.	.10	-	1.0	1.7 ± 0.1	7.0	12. ± 1.0
Optimum Slit Width (μ)[b]	30.		32.		36.	

[a] Estimated flame temperature[28] 2665. °K; hydrogen flow rate 5,000 $cm^3 min^{-1}$; oxygen flow rate 2,500 $cm^3 min^{-1}$; sample aspiration rate 1.78 $cm^3 min^{-1}$; wavelength 4227 Å; atomization efficiency factor, ϵ,[27] estimated at 0.5.

[b] Calculated optimum slit width.

TABLE 18

CALCULATED AND MEASURED SIGNAL-TO-NOISE RATIOS FOR THREE CONCENTRATIONS OF CALCIUM IN A FUEL RICH HYDROGEN-OXYGEN FLAME[a]

Concentration (ppm)	0.1		1.0		10.	
Study Slit Width (μ)	Calculated	Measured	Calculated	Measured	Calculated	Measured
30.	3.5	-	18.	17. ± 10.	47.	48. ± 10.
50.	3.8	-	19.	33. ± 13.	49.	41. ± 4.
70.	3.8	-	20.	29. ± 7.	49.	52. ± 5.
90.	3.6	-	19.	31. ± 6.	48.	44. ± 3.
110.	3.4	6.7 ± 2.	18.	28. ± 4.	48.	38. ± 2.
400.	1.5	1.4 ± 0.2	11.	16. ± 2.	36.	43. ± 5.
800.	.86	1.2 ± 0.1	8.0	11. ± 1.	30.	40. ± 3.
1000.	.68	-	6.0	8.9 ± 1.	25.	31. ± 2.
Optimum Slit Width (μ)[b]	65.		74.		75.	

[a] Estimated flame temperature[28] 2645. °K; hydrogen flow rate 10,000 cm^3min^{-1}; oxygen flow rate 2,500 cm^3min^{-1}; sample aspiration rate 1.63 cm^3min^{-1}; wavelength 4227 Å; atomization efficiency factor, ϵ,[27] estimated at 0.5.

[b] Calculated optimum slit width.

TABLE 19

CALCULATED AND MEASURED SIGNAL-TO-NOISE RATIOS FOR THREE CONCENTRATIONS OF CALCIUM IN A STOICHIOMETRIC ACETYLENE-OXYGEN FLAME[a]

Concentration (ppm)	0.1		1.0		10.	
Study Slit Width (μ)	Calculated	Measured	Calculated	Measured	Calculated	Measured
30.	.45	-	4.1	4.7 ± 1.	17.	28. ± 6.
50.	.35	-	3.2	6.7 ± 1.	15.	24. ± 2.
70.	.28	-	2.7	4.2 ± .4	14.	26. ± 3.
90.	.24	-	2.3	2.8 ± .2	12.	26. ± 2.
110.	.20	.50 ± .03	2.0	3.3 ± .2	11.	26. ± 2.
400.	.06	-	.74	1.5 ± .1	5.1	16. ± 4.
800.	.04	-	.46	.5 ± .03	3.4	6.1 ± .6
1000.	.03	-	.33	1.0 ± .1	2.5	5.7 ± .7
Optimum Slit Width (μ)[b]	10.		10.		10.	

[a] Estimated flame temperature[28] 2937. °K; acetylene flow rate 1,400. cm^3min^{-1}; oxygen flow rate 3,500. cm^3min^{-1}; sample aspiration rate 1.91 cm^3min^{-1}; wavelength 4227 Å; atomization efficiency factor, ϵ,[27] estimated at 0.5.

[b] Calculated optimum slit width.

TABLE 20

CALCULATED AND MEASURED SIGNAL-TO-NOISE RATIOS FOR THREE CONCENTRATIONS OF LITHIUM IN A STOICHIOMETRIC HYDROGEN-OXYGEN FLAME[a]

Concentration (ppm)	10.		100.		1000.	
Study Slit Width (μ)	Calculated	Measured	Calculated	Measured	Calculated	Measured
30.	5.5	13. ± 2.	13.	47. ± 3.	31.	58. ± 6.
50.	7.6	31. ± 3.	17.	45. ± 2.	36.	74. ± 9.
70.	9.2	32. ± 3.	20.	51. ± 4.	39.	63. ± 5.
90.	11.	32. ± 2.	22.	51. ± 4.	42.	57. ± 4.
110.	11.	31. ± 2.	24.	54. ± 3.	43.	67. ± 7.
400.	20.	37. ± 2.	35.	63. ± 6.0	50.	57. ± 4.
800.	23.	40. ± 4.	39.	50. ± 3.0	51.	76. ± 10.
1000.	23.	31. ± 2.	39.	67. ± 9.	51.	57. ± 5.
Optimum Slit Width (μ)[b]	970.		1000.		1000.	

---

[a] Estimated flame temperature[28] 2665 °K; hydrogen flow rate 5,000. cm^3min^{-1}; oxygen flow rate 2,500. cm^3min^{-1}; sample aspiration rate 1.50 cm^3min^{-1}; wavelength 6708 Å; atomization efficiency factor, ϵ,[27] estimated at 0.5.

[b] Calculated optimum slit width.

TABLE 21

CALCULATED AND MEASURED SIGNAL-TO-NOISE RATIOS FOR THREE CONCENTRATIONS OF LITHIUM IN A FUEL RICH HYDROGEN-OXYGEN FLAME[a]

Concentration (ppm)	10.		100.		1000.	
Study Slit Width (µ)	Calculated	Measured	Calculated	Measured	Calculated	Measured
30.	7.2	33. ± 2.	15.	57. ± 5.	23.	72. ± 6.
50.	9.8	57. ± 6.	20.	93. ± 11.	29.	89. ± 9.
70.	12.	60. ± 6.	23.	103. ± 15.	33.	84. ± 10.
90.	14.	53. ± 3.	26.	94. ± 12.	36.	86. ± 10.
110.	15.	66. ± 9.	29.	81. ± 9.	39.	83. ± 8.
400.	25.	58. ± 6.	44.	104. ± 20.	55.	130. ± 32.
800.	27.	60. ± 9.	47.	96. ± 13.	58.	83. ± 9.
1000.	27.	38. ± 4.	48.	-	60.	61. ± 4.
Optimum Slit Width (µ)[b]	800.		930.		999.	

[a] Estimated flame temperature[28] 2645 °K; hydrogen flow rate 10,000. cm^3min^{-1}; oxygen flow rate 2,500. cm^3min^{-1}; sample aspiration rate 1.47 cm^3min^{-1}; wavelength 6708 Å; atomization efficiency factor, ϵ,[27] estimated at 0.5.

[b] Calculated optimum slit width.

TABLE 22

CALCULATED AND MEASURED SIGNAL-TO-NOISE RATIOS FOR THREE CONCENTRATIONS OF LITHIUM IN A STOICHIOMETRIC ACETYLENE-OXYGEN FLAME[a]

Concentration (ppm)	10.		100.		1000.	
Study	Calculated	Measured	Calculated	Measured	Calculated	Measured
Slit Width (μ)						
30.	9.2	86. ± 11.	18.	68. ± 7.	25.	30. ± 2.
50.	9.2	122. ± 24.	18.	83. ± 10.	25.	40. ± 2.
70.	9.1	85. ± 9.	18.	72. ± 6.	25.	52. ± 6.
90.	8.5	98. ± 10.	17.	88. ± 14.	24.	43. ± 3.
110.	8.2	97. ± 15.	17.	83. ± 11.	24.	44. ± 3.
400.	3.7	104. ± 16.	10.	69. ± 7.	16.	46. ± 6.
800.	2.4	76. ± 6.	7.	84. ± 13.	12.	29. ± 4.
1000.	1.8	116. ± 23.	5.	58. ± 6.	10.	16. ± 1.
Optimum Slit Width[b] (μ)	47.		49.		50.	

[a] Estimated flame temperature[28] 2937. °K; acetylene flow rate 1,400. cm^3min^{-1}; oxygen flow rate 3,500. cm^3min^{-1}; sample aspiration rate 1.88 cm^3min^{-1}; wavelength 6708 Å; atomization efficiency factor, ϵ,[27] estimated at 0.5.

[b] Calculated optimum slit width.

TABLE 23

CALCULATED AND MEASURED SIGNAL-TO-NOISE RATIOS FOR THREE CONCENTRATIONS OF SODIUM IN A STOICHIOMETRIC HYDROGEN-OXYGEN FLAME[a]

Concentration (ppm)	0.1		1.0		10.	
Study Slit Width (μ)	Calculated	Measured	Calculated	Measured	Calculated	Measured
30.	13.	30. ± 2.	22.	30. ± 2.	47.	55. ± 4.
50.	16.	40. ± 2.	37.	46. ± 4.	49.	43. ± 3.
70.	18.	48. ± 5.	39.	49. ± 3.	50.	48. ± 3.
90.	19.	43. ± 3.	40.	54. ± 6.	50.	61. ± 7.
110.	21.	40. ± 3.	41.	50. ± 5.	50.	52. ± 5.
400.	23.	41. ± 2.	44.	45. ± 3.	51.	49. ± 4.
800.	22.	47. ± 4.	43.	50. ± 3.	51.	80. ± 7.
1000.	18.	38. ± 2.	41.	48. ± 4.	50.	90. ± 17.
Optimum Slit Width (μ)[b]	270.		320.		330.	

[a] Estimated flame temperature[28] 2665. °K; hydrogen flow rate 5,000. $cm^3 min^{-1}$; oxygen flow rate 2,500. $cm^3 min^{-1}$; sample aspiration rate 1.60 $cm^3 min^{-1}$; wavelength 5890 Å; atomization efficiency factor, ϵ,[27] estimated at 0.5.

[b] Calculated optimum slit width.

TABLE 24

CALCULATED AND MEASURED SIGNAL-TO-NOISE RATIOS FOR THREE CONCENTRATIONS OF SODIUM IN A FUEL RICH HYDROGEN-OXYGEN FLAME[a]

Concentration (ppm)	0.1		1.0		10.	
Study Slit Width (µ)	Calculated	Measured	Calculated	Measured	Calculated	Measured
30.	12.	52. ± 4.	39.	86. ± 12.	64.	128. ± 28.
50.	16.	68. ± 8.	44.	107. ± 18.	67.	94. ± 9.
70.	18.	70. ± 7.	48.	90. ± 11.	69.	98. ± 14.
90.	20.	76. ± 14.	51.	83. ± 8.	70.	130. ± 22.
110.	23.	87. ± 15.	53.	150. ± 43.	70.	108. ± 14.
400.	34.	57. ± 6.	60.	184. ± 53.	74.	109. ± 15.
800.	37.	75. ± 13.	65.	91. ± 11.	74.	206. ± 89.
1000.	37.	80. ± 14.	66.	74. ± 7.	74.	107. ± 21.
Optimum Slit Width (µ)[b]	810.		960.		990.	

[a] Estimated flame temperature[28] 2645. °K; hydrogen flow rate 10,000. $cm^3 min^{-1}$; oxygen flow rate 2,500. $cm^3 min^{-1}$; sample aspiration rate 1.54 $cm^3 min^{-1}$; wavelength 5890 Å; atomization efficiency factor, ϵ ,[27] estimated at 0.5.

[b] Calculated optimum slit width.

TABLE 25

CALCULATED AND MEASURED SIGNAL-TO-NOISE RATIOS FOR THREE CONCENTRATIONS OF SODIUM IN A STOICHIOMETRIC ACETYLENE-OXYGEN FLAME[a]

Concentration (ppm)	0.1		1.0		10.	
Study Slit Width (μ)	Calculated	Measured	Calculated	Measured	Calculated	Measured
30.	18.	34. ± 3.	33.	90. ± 12.	35.	87. ± 12.
50.	19.	24. ± 1.	33.	75. ± 11.	35.	84. ± 13.
70.	21.	33. ± 3.	33.	72. ± 7.	35.	86. ± 11.
90.	21.	32. ± 3.	34.	88. ± 10.	35.	78. ± 8.
110.	21.	29. ± 2.	34.	119. ± 24.	35.	95. ± 10.
400.	12.	14. ± 1.	33.	74. ± 11.	35.	77. ± 7.
800.	5.0	11. ± 1.	32.	105. ± 35.	34.	82. ± 12.
1000.	2.0	7.0± 1.	31.	42. ± 5.	34.	93. ± 12.
Optimum Slit Width (μ)[b]	11.		11.		11.	

[a] Estimated flame temperature[28] 2937. °K; acetylene flow rate 1,400. cm^3min^{-1}; oxygen flow rate 3,500. cm^3min^{-1}; sample aspiration rate 1.81 cm^3min^{-1}; wavelength 5890 Å; atomization efficiency factor, ϵ,[27] estimated at 0.5.

[b] Calculated optimum slit width.

TABLE 26

CALCULATED AND MEASURED SIGNAL-TO-NOISE RATIOS FOR THREE CONCENTRATIONS OF STRONTIUM IN A STOICHIOMETRIC HYDROGEN-OXYGEN FLAME[a]

Concentration (ppm)	1.0		10.		100.	
Study Slit Width (μ)	Calculated	Measured	Calculated	Measured	Calculated	Measured
30.	13.	-	33.	10. ± 2.	48.	35. ± 4.
50.	12.	-	32.	16. ± 2.	47.	41. ± 3.
70.	11.	-	31.	19. ± 1.	47.	45. ± 4.
90.	10.	-	30.	21. ± 1.	46.	45. ± 3.
110.	9.0	-	29.	25. ± 2.	46.	47. ± 3.
400.	4.2	-	18.	40. ± 4.	38.	36. ± 3.
800.	2.7	-	14.	22. ± 2.	33.	39. ± 2.
1000.	2.0	-	12.	16. ± 2.	30.	42. ± 3.
Optimum Slit Width (μ)[b]	25.		25.		27.	

---

[a] Estimated flame temperature[28] 2665. °K; hydrogen flow rate 5,000. $cm^3 min^{-1}$; oxygen flow rate 2,500. $cm^3 min^{-1}$; sample aspiration rate 1.58 $cm^3 min^{-1}$; wavelength 4601 Å; atomization efficiency factor, ϵ,[27] estimated at 0.5.

[b] Calculated optimum slit width.

TABLE 27

CALCULATED AND MEASURED SIGNAL-TO-NOISE RATIOS FOR THREE CONCENTRATIONS OF STRONTIUM IN A FUEL RICH HYDROGEN-OXYGEN FLAME[a]

Concentration (ppm)	1.0		10.		100.	
Study Slit Width (µ)	Calculated	Measured	Calculated	Measured	Calculated	Measured
30.	25.	9. ± 1.	68.	31. ± 2.	74.	66. ± 8.
50.	25.	13. ± 1.	69.	48. ± 5.	74.	63. ± 6.
70.	24.	17. ± 1.	68.	45. ± 3.	74.	60. ± 4.
90.	23.	21. ± 2.	68.	58. ± 6.	74.	56. ± 5.
110.	22.	23. ± 2.	67.	55. ± 4.	73.	61. ± 6.
400.	12.	20. ± 3.	56.	58. ± 7.	70.	95. ± 18.
800.	9.	13. ± 2.	48.	43. ± 3.	66.	75. ± 8.
1000.	7.	9. ± 1.	42.	52. ± 8.	63.	38. ± 2.
Optimum Slit Width (µ)[b]	42.		50.		50.	

[a] Estimated flame temperature[28] 2645. °K; hydrogen flow rate 10,000. $cm^3 min^{-1}$; oxygen flow rate 2,500. $cm^3 min^{-1}$; sample aspiration rate 1.47 $cm^3 min^{-1}$; wavelength 4601 Å; atomization efficiency factor, ϵ ,[27] estimated at 0.5.

[b] Calculated optimum slit width.

TABLE 28

CALCULATED AND MEASURED SIGNAL-TO-NOISE RATIOS FOR THREE CONCENTRATIONS OF STRONTIUM IN A STOICHIOMETRIC ACETYLENE-OXYGEN FLAME[a]

Concentration (ppm)	1.0		10.		100.	
Study Slit Width (µ)	Calculated	Measured	Calculated	Measured	Calculated	Measured
30.	7.3	-	22.	-	33.	12. ± 1.
50.	5.9	-	21.	3.7 ± .3	32.	23. ± 1.
70.	5.2	-	20.	4.4 ± .3	32.	28. ± 2.
90.	4.4	-	19.	5.5 ± .3	31.	32. ± 3.
110.	4.0	-	18.	8.9 ± .7	30.	31. ± 2.
400.	1.6	-	12.	4.7 ± .3	25.	35. ± 3.
800.	1.0	-	9.1	3.5 ± .3	22.	22. ± 2.
1000.	.67	-	7.5	1.8 ± .2	19.	18. ± 1.
Optimum Slit Width (µ)[b]	10.		10.		10.	

[a] Estimated flame temperature[28] 2937. °K; acetylene flow rate 1,400. cm^3min^{-1}; oxygen flow rate 3,500. cm^3min^{-1}; sample aspiration rate 1.89 cm^3min^{-1}; wavelength 4601 Å; atomization efficiency factor, ϵ,[27] estimated at 0.5.

[b] Calculated optimum slit width.

agreement between curve shapes and magnitude was not exact but certain conclusions can nevertheless be drawn from a comparison of the calculated and measured values and curve shapes. For one thing the calculated curves predict, and the measured curves bear out (see Tables 21,22,23,24,25) that the signal-to-noise ratio for low concentrations is dependent on slit width whereas it is independent of slit width for high concentrations over a wide range of slit width values. Other conclusions to be drawn from a comparison of the calculated and measured curves are not as immediately obvious, but these will be pointed out in the following paragraphs.

If Equation (17) is used to study the effect of individual parameters, then, for low sample concentrations, quite accurate values for the two flame parameters, I_c and ψ must be known in order to predict accurately the shape of the signal-to-noise ratio versus slit width curves (see Figures 5 and 6). To predict the magnitude of the signal-to-noise ratio, an accurate value of Δf must also be known. The effect of I_c diminishes as the sample concentration increases, but the effect of ψ is felt at all concentrations and is more significant anyway. In this study, a single value was assigned to ψ for each flame type. That value was based on average readings made in this study. However, the complete series of measurements covered a number of days and the possibility exists that the flicker factor value did not remain constant for each type of flame for that long. If it is assumed that ψ has an incorrect value, then a disagreement would be expected, in the shape and position, between the calculated and measured curves of signal-to-noise ratio plotted against slit width. The general characteristics of the two sets of curves would still be the same; they would all start at the origin, rise to some maximum height, and then either level off or drop slightly for high concentrations. Any deviation from theory would fall into one of three patterns: (a) for those measurements in which the actual value of ψ was greater than the assumed value of ψ , the calculated curve would be in general higher than the measured curve, and the maximum of the calculated curve would be to the right (wider slit widths) of the maximum of the measured curve; (b) for those measurements in which the actual value of ψ is less than the assumed value of ψ , the calculated curve would in general be lower than the measured curve and the maximum of the calculated curve would be to the left (narrower slit widths) of the maximum of the measured curve; (c) for those measurements in which the actual and the assumed values of are approximately equal, there would be general agreement between the two curves. If only a portion of the complete signal-to-noise ratio versus slit width curve was either calculated or measured (as was the case sometimes in this study) then the maximum might fall outside of the plotted portion and the location of the maximum would have to be estimated by the slope of that portion of whichever leg of the curve appears in the plot. It should also be expected that inaccuracies in I_c and Δf values would alter the curve shapes to some extent, but the curve shapes should still be discernable because the influence of ψ should predominate.

A complete listing of the calculated signal-to-noise ratio values and their corresponding measured values is given in Tables 14 through 28. As expected, the reasons for disagreement between theory and experiment are not entirely clear in all cases. Representative plots of signal-to-noise ratio versus slit width are given in Figures 2, 3, and 4. In Figure 2, the calculated and measured signal-to-noise ratio versus slit width curves for the 0.1 ppm sodium solution in the stoichiometric acetylene-oxygen flame are compared. This is considered to be a case in which the assumed value of ψ is smaller than the actual value of ψ, because the maximum of the calculated curve is to the right of the maximum of the measured curve. Figure 3 compares the calculated and measured signal-to-noise ratio versus slit width curves for the 1000 ppm lithium solution in the stoichiometric acetylene-oxygen flame. This

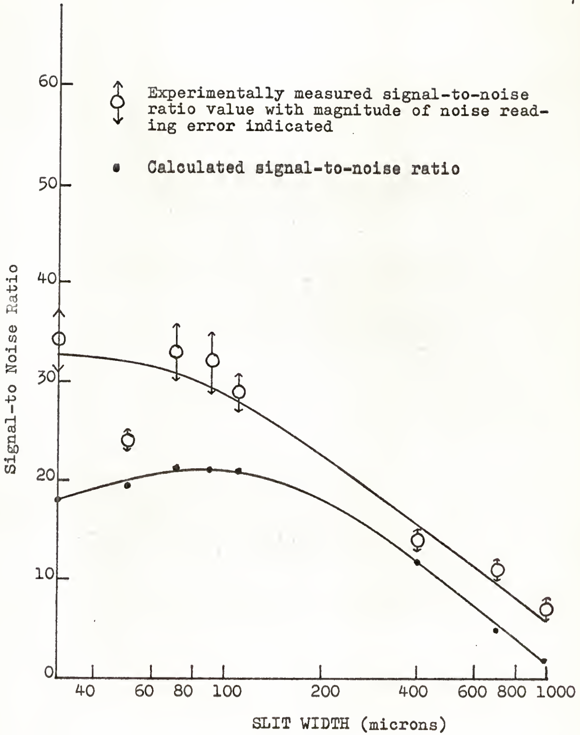

Fig. 2.-Comparison of theoretical and experimental signal-to-noise ratio versus slit width curves for a 0.1 ppm sodium (5890 Å) solution in a stoichiometric acetylene-oxygen flame.

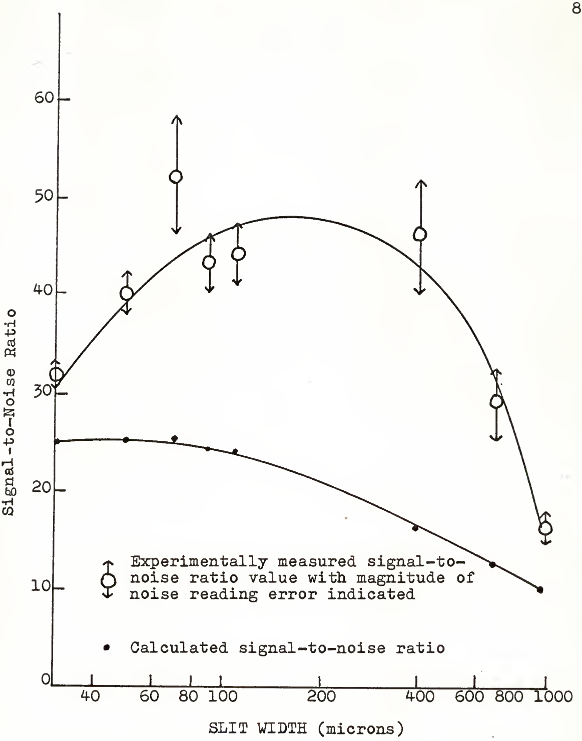

Fig. 3.-Comparison of theoretical and experimental signal-to-noise ratio versus slit width curves for a 1000 ppm lithium (6708 Å) solution in a stoichiometric acetylene-oxygen flame.

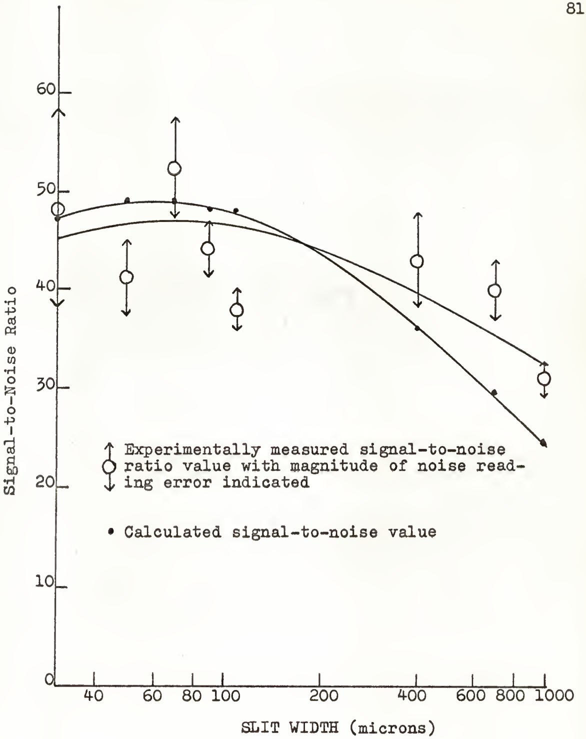

Fig. 4.-Comparison of theoretical and experimental signal-to-noise ratio versus slit width curves for a 10 ppm calcium (4227 Å) solution in a fuel rich hydrogen-oxygen flame.

is considered to be a case in which the assumed value of is greater than the actual value of ψ , because the maximum of the calculated curve is to the left of the maximum of the measured curve. Figure 4 compares the calculated and measured signal-to-noise ratio versus slit width curves for the 100 ppm solution of calcium in the fuel rich hydrogen-oxygen flame. This is considered to be a case in which the assumed and the actual values of ψ are approximately equal, because of the general agreement between the two curves. The majority of the comparisons seem to be of the type that indicate an assumed value of ψ that is greater than the actual value of ψ .

The above results can be summarized as follows: if the value of ψ is too variable to be presented in Equation (17) as a single value over a series of measurements, then Equation (17) would indicate a disagreement between calculated and measured signal-to-noise ratio versus slit width curves. The agreement between calculated and measured signal-to-noise ratios indicates that Equation (17) is valid, as has been shown by other uses to which essentially the same equation has been put by Vickers.[25] Furthermore, it can be assumed that the flame flicker factor, ψ , is a parameter whose value is not constant enough such that a single value can be assumed for it throughout a lengthy series of measurements.

V. INFLUENCE ON SIGNAL-TO-NOISE RATIO VERSUS SLIT WIDTH CURVES OF INDEPENDENTLY VARYING INDIVIDUAL PARAMETERS

The relative significance of each of the instrumental parameters of Equation (17) can be found by use of the computer program for calculating points on the signal-to-noise ratio versus slit width curve. The evaluation of parameters used in Equation (17) has already been discussed. Using these values, the calculated points on the signal-to-noise ratio versus slit width curve should produce a curve of the same shape as that measured experimentally, that is, a normal curve should result. Those values for each parameter, which were considered to be valid for sodium in the stoichiometric acetylene-oxygen flame, were arbitrarily considered to be normal for this portion of the study and were used in Equation (17). To alter any single one of these values (while holding the rest at their estimated normal value) should produce an abnormally shaped curve. The relative deviation of the abnormal curve from the normal curve should be a measure of the relative significance of that parameter to the value of the signal-to-noise ratio. Such information could be of value to further theoretical studies in flame spectrometry.

The relative significance of each parameter might be predicted from Equation (17) by purely algebraic means. However the availability of the computer program, and the ease with which each parameter's value can be increased or decreased, with a complete set of curve points produced for each variation of a parameter, makes this sort of investigation uniquely appropriate to this study. Consequently each of the following parameters (or parameter combinations), ψ, I_c, i_d, γ and M, was increased threefold and decreased threefold while all of the other parameters were held at their estimated normal value. The parameter W_m was felt to be subject to less drastic fluctuations, and so it would be more useful to observe the effect of a twofold increase and decrease from its estimated normal value of .003 cm (estimated from Herrmann and Alkemade[8]). The resulting distortions in the shape of the signal-to-noise ratio versus slit width curves for each parameter are shown in Figures 5, 6, 7, 8, and 9. Several conclusions can be drawn from the shapes of the curves.

In general, wider slit widths increase the signal-to-noise ratio.

At low concentrations the signal-to-noise ratio versus slit width curves show a sharper maximum. At high concentrations the signal-to-noise ratio reaches a maximum value, levels off, and is virtually independent of slit widths.

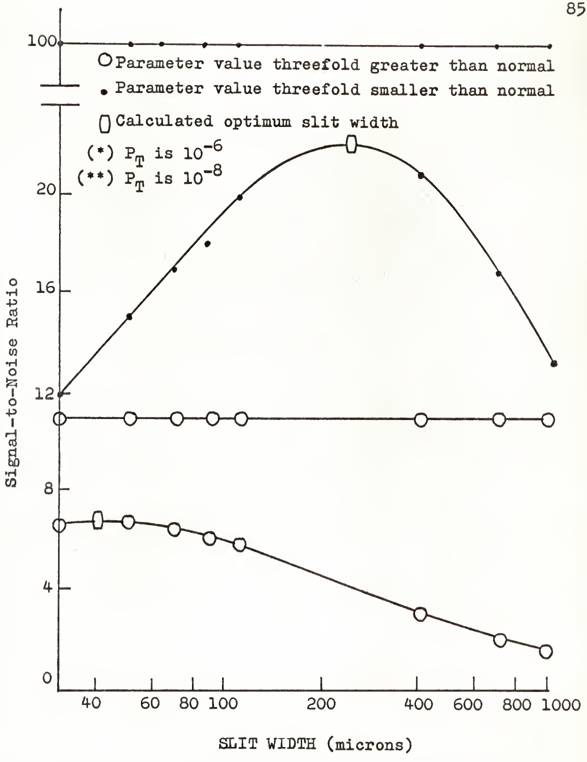

Fig. 5.-Signal-to-noise ratio versus slit width curves for extreme values of the flame flicker factor.

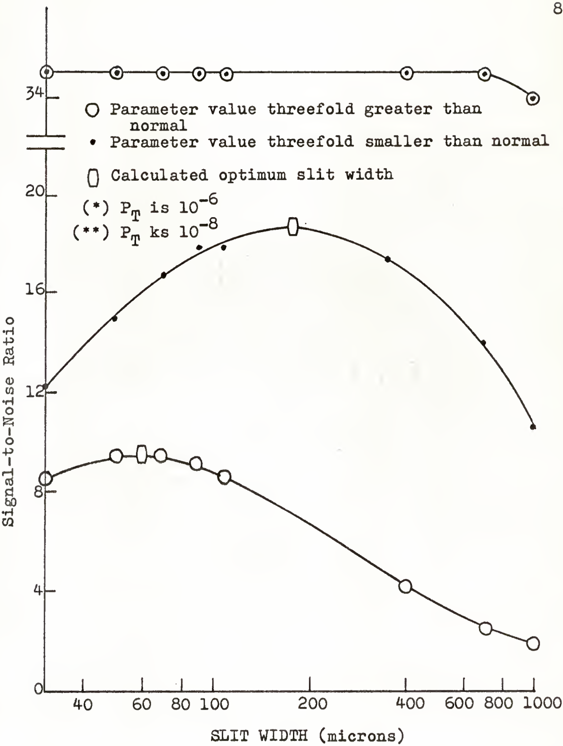

Fig. 6.-Signal-to-noise ratio versus slit width curves for extreme values of the continuum intensity.

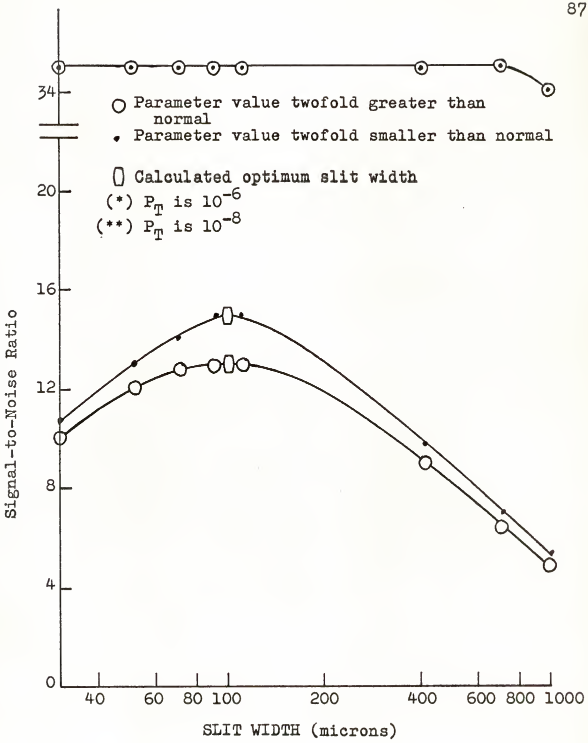

Fig. 7.-Signal-to-noise ratio versus slit width curves for extreme values of the minimum resolving power slit width.

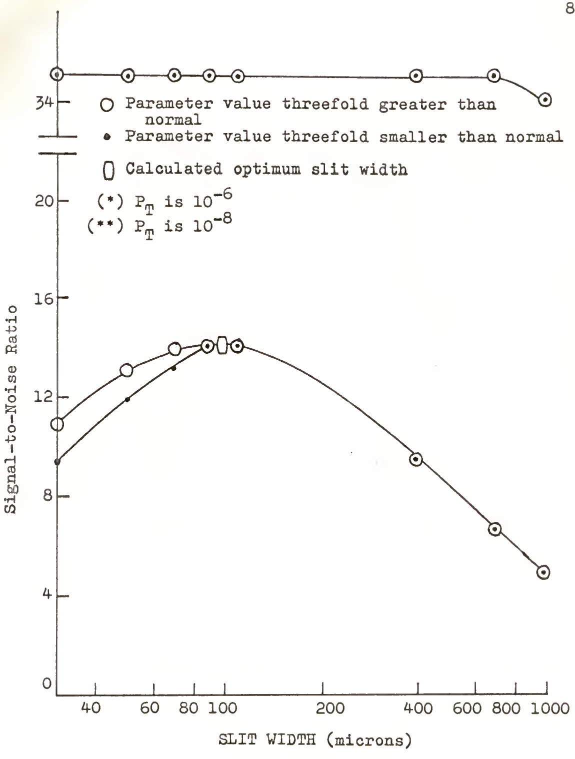

Fig. 8.-Signal-to-noise ratio versus slit width curves for extreme values of the photosensitivity factor and the photomultiplier tube gain factor.

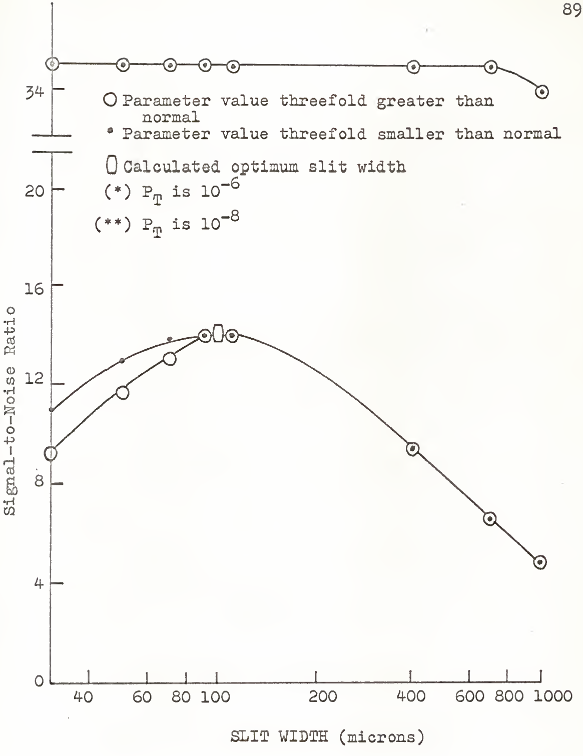

Fig. 9.-Signal-to-noise ratio versus slit width curves for extreme values of the photoanodic dark current.

The flame flicker parameter has the greatest effect on the magnitude of the signal-to-noise ratio of any of the parameters studied. It is the flicker factor (along with Δf) which determines the value of the high concentration maximum (see Eqn. (40)).

Increasing the γ and M factors causes a slight increase in signal-to-noise ratio that can be observed for low sample concentrations at slit widths below the optimum. This indicates that increased sensitivity amplifies the signal somewhat more than it amplifies the noise, at least at narrow slit widths.

Larger values for the photoanodic dark current, which results in larger instrumental noise, has the greatest effect at narrow slit width and low concentration.

It is interesting to note that a given increase in the photoanodic dark current, i_d, will cause a similar change in the curve that would result from an identical decrease in the photomultiplier tube gain factors, γ and M.

In general, instrumental noises are significant at narrow slit widths, and flame noises are predominant at normal or wide slit widths.

The only parameter which greatly influences signal-to-noise ratio as slit widths increase is the continuum intensity. Opening the slit wider increases the continuum's proportion of the total intensity entering the instrument.

This is because increasing the slit also increases the spectral band width. Consequently Equation (40) in which it is assumed that the continuum intensity had become insignificant, is no longer valid, and the horizontal curve at the maximum, which it predicts, does not occur. Rather the equation which does apply is

$$i/\overline{\Delta i}_T = I/\Delta f^{1/2} \psi \, [I_c R_d (W+W_m)+I] \qquad (43)$$

and the signal-to-noise ratio will decrease with increasing slit widths.

The two flame parameters, continuum intensity and the flame flicker factor, and the shot noise term control the value of the optimum slit width, that is, the location of the maximum of the signal-to-noise ratio versus slit width curve. At low values for I_c its depressing influence is delayed, and the maximum occurs at wider slits. When I_c is large, its depressing influence is felt at narrower slits so the optimum slit width is smaller. The flicker factor controls the proportion of noise that accompanies the continuum intensity, and so, for a given I_c, higher values of ψ would have the same result that a higher value of I_c would have. Consequently large values for either I_c, or ψ, or both, tend to cause the optimum slit width to be narrower; small values for either I_c, or ψ, or both, tend to cause the optimum slit width to be larger.

The difference in shape between the high and low concentration signal-to-noise ratio versus slit width curves is due to the relative sizes of spectral line intensity and continuum intensity. Continuum intensity is approximately constant, but spectral line intensity, of course, varies with sample concentration. If the spectral line intensity is high, the continuum intensity will be insignificant, and Equation (40) will control the shape of the curve until very wide slit widths are reached, at which point Equation (43) will be valid and the curve will begin to drop. If the spectral line intensity is low, Equation (43) will become valid at much narrower slit widths, and there will not be a broad flat maximum to the curve.

VI. SUMMARY OF CONCLUSIONS

1. Decreasing flame noises offers more promise of improving the signal-to-noise ratio than decreasing instrument noises. However narrower frequency response band widths will improve the ratio.

2. A decrease in the flame flicker noise results in the greatest improvement in the signal-to-noise ratio.

3. The flame flicker factor does not have a sufficiently constant value such that a single value for it could be assumed, even in a given flame, over an extended period of measurements. If values for this parameter are required, they should be obtained frequently by measuring the signal-to-noise ratio of a high concentration sample.

4. All other things being equal, better signal-to-noise ratios result with wider slit widths; but extremely wide slits will always lower the signal-to-noise ratio value.

5. Slit widths are critical at low sample concentrations but are much less so at higher sample concentrations.

6. Instrument noises are significant at slit widths narrower than the optimum slit whereas flame noises predominate at slit widths wider than the optimum slit.

7. At slit widths larger than the optimum slit width changes in sensitivity setting, that is, gain factor of the phototube, have no effect on the signal-to-noise ratio.

8. For studies in regions in which the flame continuum intensity is higher narrower optimum slit widths result than for regions of lower flame continuum intensity.

9. When using less stable flames narrower optimum slit widths result than with more stable flames.

APPENDICES

APPENDIX 1

Fortran Program for Calculating the Total Partial Pressure of the Metal in the Various Forms Present in the Flame Gases as a Function of Flame Type. Molar Concentration of the Aspirated Solution, and the Aspiration Rate-Efficiency Factor Product.

This program is designed to calculate, in atmospheres, the sum of the partial pressures of all forms of the metal element that are present in the flame gases. The parameter, P_T, is used in a later program for calculating the number of uncombined metal atoms present per cm^3 of flame gases. The calculations performed by the programs are based on the equation given by Vickers[24]

$$P_T = 3. \times 10^{21} k(\Phi\, n_{298}/Q n_T)\, \epsilon\, C \quad , \qquad (44)$$

where k is the Boltzmann constant in cm^3 atm $^{o}K^{-1}$, Φ is the aspiration rate in cm^3 min^{-1}, n_{298} and n_T are the moles of gases present before combustion and the moles of gases present after combustion respectively. (In both cases, the moles of aspirated solution are included and the volume units are the same.) The factor Q is the flow rate of unburned gases in cm^3 atm $^{o}K^{-1}$, ϵ is the atomization efficiency factor applied to the aspiration rate[27] and

C is the concentration of the aspirated solution in moles liter^{-1}. By the proper choice of units for n_{298}, it can be made equal to Q. Then Equation (44) reduces to

$$P_T = 0.414(\Phi\epsilon/n_T)C \qquad (45)$$

Both of the terms, $\Phi\epsilon$ and C, are independent parameters while n_T depends upon the types of fuel and oxygen and on their ratio.

The data used in this program consists of arbitrary values for fuel flow rate, oxygen (or air) flow rate, molar concentration of aspirated solution, and aspiration rate--efficiency factor product. By means of this program P_T values are calculated for various solution concentrations being aspirated at various rates into flames that vary both as to types of fuel and oxygen and as to ratios of fuel to oxygen flow rates. A computed GO TO statement allows the program to select a different subroutine for each type of fuel-oxygen combination. A GO TO 1 statement makes it possible to use separate decks of data cards for different ranges of fuel flow rates because the flow rates used for hydrogen are quite different than those used for acetylene. An IF statement within the subroutine allows for the selection of different arithmetic statements for each of the three possible situations of the flame: fuel rich, stoichiometric, or oxygen rich. The interpretation of terms used in the program is as follows:

FUEL(J)	Flow rate of fuel gas in cm^3 sec^{-1}.
XFUEL(J)	Flow rate of fuel gas in cm^3 min^{-1}.
OX(K)	Flow rate of oxygen or air in cm^3 sec^{-1}.
XOX(K)	Flow rate of oxygen or air in cm^3 min^{-1}.
PHEC(L)	Product of aspiration rate, in cm^3 min^{-1} and the efficiency factor.
C(M)	Molar concentration of the aspirated solution.
PT(L,M)	Total (partial) pressure of the metal species, in all its forms, present in the flame gases, in atmospheres.
JJ	Limit of the list of fuel flow rates.
KK	Limit of the list of oxygen flow rates.
LL	Limit of the list of aspiration rate-efficiency factor product values.
MM	Limit of the list of solution concentrations.
JJJ	Lower index limit of loop involving computed GO TO.
KKK	Upper index limit of loop involving computed GO TO.
A	Surplus fuel gas, after combustion, in cm^3 sec^{-1}.
B	Surplus oxygen, after combustion, in cm^3 sec^{-1}.
D	Water vapor in the combustion products in cm^3 sec^{-1}.
C	Carbon dioxide in the combustion products in cm^3 sec^{-1}.
H	Nitrogen in cm^3 sec^{-1}.
XX	Sum of the combustion product gases in cm^3 sec^{-1}.

The composition of the data deck (assuming 6 values for the flow rates of both fuel and oxygen, 10 values for PHEC, and 8 values for concentration) are as follows:

```
JJ        KK        LL        MM         JJJ       KKK
FUEL(1)   FUEL(2)   FUEL(3)   FUEL(4)    FUEL(5)   FUEL(6)
OX(1)     OX(2)     OX(3)     OX(4)      OX(5)     OX(6)
PHEC(1)   PHEC(2)   PHEC(3)   PHEC(4)    PHEC(5)   PHEC(6)
PHEC(7)   PHEC(8)   PHEC(9)   PHEC(10)   C(1)      C(2)
C(3)      C(4)      C(5)      C(6)       C(7)      C(8)
```

An example of the way the computed values are printed is as follows:

```
                      HYDROGEN/OXYGEN FLAME

Fuel Flow Rate 3000 CC/Min
OXYGEN FLOW RATE 500 CC/MIN

LOG CONC. MOLES/LITER       -10     -9     -8     ....     ....

ASP. RATE X EFF. FAC. CC/MIN

            0.20
            0.40
            0.60    (P_T values)
            ...
            ...
```

The Fortran program itself is as follows:

```
      DIMENSION FUEL(6),OX(6),PHEC(10),C(8),PT(10,8)
    1 READ INPUT TAPE 5,100,JJ,KK,LL,MM,JJJ,KKK,(FUEL(J),J=1
     1,JJ),(OX(K),K=1,KK),(PHEC(L),L=1,LL),(C(M),M=1,MM)
      WRITE OUTPUT TAPE 6,101,JJ,KK,LL,MM,JJJ,KKK,(FUEL(J),J
     1=1,JJ),(OX(K),K=1,KK),(PHEC(L),L=1,LL),(C(M),M=1,MM)
  100 FORMAT (6I12/(6E12.2))
  101 FORMAT (1H2,6I12/(6E12.2))
      DO 50 I=JJJ,KKK
      GO TO (10,20,30,40),I
   10 DO 18 J=1,JJ
      DO 18 K=1,KK
      IF (.5*FUEL(J)-OX(K))11,12,13
   11 A=0.
      B=OX(K)-.5*FUEL(J)
      D=FUEL(J)
      GO TO 14
   12 A=0.
      B=0.
      D=FUEL(J)
      GO TO 14
   13 A=FUEL(J)-2.*OX(K)
      B=0.
      D=2.*OX(K)
   14 XX=A+B+D
      DO 15 L=1,LL
      DO 15 M=1,MM
   15 PT(L,M)=(.424*PHEC(L)*C(M))/(XX+(22.5*PHEC(L)))
      XFUEL=60.*FUEL(J)
      XOX=60.*OX(K)
      WRITE OUTPUT TAPE 6,102
  102 FORMAT (1H1,49X,21HHYDROGEN/OXYGEN FLAME)
      WRITE OUTPUT TAPE 6,103,XFUEL,XOX
      DO 16 L=1,LL
      WRITE OUTPUT TAPE 6,104,PHEC(L),(PT(L,M),M=1,MM)
   16 CONTINUE
   18 CONTINUE
```

```
      GO TO 50
   20 DO 28 J=1,JJ
      DO 28 K=1,KK
      IF(.5*FUEL(J)-.2*OX(K))21,22,23
   21 A=0.
      B=.2*OX(K)-.5*FUEL(J)
      D=.5*FUEL(J)
      H=.8*OX(K)
      GO TO 24
   22 A=0.
      B=0.
      D=FUEL(J)
      H=.4*OX(K)
      GO TO 24
   23 A=FUEL(J)-.4*OX(K)
      B=0.
      D=.4*OX(K)
      H=.8*OX(K)
   24 XX=A+B+D+H
      DO 25 L=1,LL
      DO 25 M=1,MM
   25 PT(L,M)=(.424*PHEC(L)*C(M))/(XX+(22.5*PHEC(L)))
      XFUEL=60.*FUEL(J)
      XOX=60.*OX(K)
      WRITE OUTPUT TAPE 6,105
  105 FORMAT (1H1,51X,18HHYDROGEN/AIR FLAME)
      WRITE OUTPUT TAPE 6,106,XFUEL,XOX
      DO 26 L=1,LL
      WRITE OUTPUT TAPE 6,104,PHEC(L),(PT(L,M),M=1,MM)
   26 CONTINUE
   28 CONTINUE
      GO TO 50
   30 DO 38 J=1,JJ
      DO 38 K=1,KK
      IF (FUEL(J)-.4*OX(K))31,32,33
   31 A=0.
```

```
      B=OX(K)-2.5*FUEL(J)
      G=2.*FUEL(J)
      D=FUEL(J)
      GO TO 34
   32 A=0.
      B=0.
      G=2.*FUEL(J)
      D=FUEL(J)
      GO TO 34
   33 A=FUEL(J)-.4*OX(K)
      B=0.
      G=2.*(FUEL(J)-A)
      D=FUEL(J)-A
   34 XX=A+B+G+D
      DO 35 L=1,LL
      DO 35 M=1,MM
   35 PT(L,M)=(.424*PHEC(L)*C(M))/(XX+(22.5*PHEC(L)))
      XFUEL=60.*FUEL(J)
      XOX=60.*OX(K)
      WRITE OUTPUT TAPE 6,107
  107 FORMAT (1H1,49X,22HACETYLENE/OXYGEN FLAME)
      WRITE OUTPUT TAPE 6,103,XFUEL,XOX
      DO 36 L=1,LL
      WRITE OUTPUT TAPE 6,104,PHEC(L),(PT(L,M),M=1,MM)
   36 CONTINUE
   38 CONTINUE
      GO TO 50
   40 DO 48 J=1,JJ
      DO 48 K=1,KK
      IF (FUEL(J)-.08*OX(K))41,42,43
   41 A=0.
      B=OX(K)-12.5*FUEL(J)
      G=2.*FUEL(J)
      D=FUEL(J)
      H=.8*OX(K)
      GO TO 44
```

```
 42 A=0.
    B=0.
    G=2.*FUEL(J)
    D=FUEL(J)
    H=.8*OX(K)
    GO TO 44
 43 A=FUEL(J)-.08*OX(K)
    B=0.
    G=2.*(FUEL(J)-A)
    D=FUEL(J)-A
    H=.8*OX(K)
 44 XX=A+B+D+G+H
    DO 45 L=1,LL
    DO 45 M=1,MM
 45 PT(L,M)=(.424*PHEC(L)*C(M))/(XX+(22.5*PHEC(L)))
    XFUEL=60.*FUEL(J)
    XOX=60.*OX(K)
    WRITE OUTPUT TAPE 6,108
108 FORMAT (1H1,50X,19HACETYLENE/AIR FLAME)
    WRITE OUTPUT TAPE 6,106,XFUEL,XOX
    DO 46 L=1,LL
    WRITE OUTPUT TAPE 6,104,PHEC(L),(PT(L,M),M=1,MM)
 46 CONTINUE
 48 CONTINUE
    GO TO 50
 50 CONTINUE
    GO TO 1
103 FORMAT (1H0,3X,14HFUEL FLOW RATE,4X,1F8.2,2X,6HCC/MIN/
   104X,16HOXYGEN FLOW RATE,2X,1F8.2(2X,6HCC/MIN///3X,21HL
   1OG CONC. MOLES/LITER,5X,3H-10,9X,10X,2H-8,10X,2H-7,10X
   1,2H-6,10X,2H-5,10X,2H-4,10X,2H-3//3X,28HASP. RATE X EF
   1F. FAC. CC/MIN)
106 FORMAT (1H0,3X,14HFUEL FLOW RATE,4X,1F8.2,2X,6HCC/MIN/
   1/4X,16HAIR FLOW RATE.2X,1F8.2,2X,6HCC/MIN///3X,21HLOG
   1CONC. MOLES/LITER,5X,3H-10,9X,2H-9,10X,2H-8,10X,2H-7,1
   10X,2H-6,10X,2H-5,10X,2H-4,10X,2H-3//3X,28HASP. RATE X
```

```
    1EFF. FAC. CC/MIN)
104 FORMAT (1H0,5X,1F12.2,6X,8E12.2)
     END
```

APPENDIX 2

Fortran Programs for Calculating the Number of Metal Atoms Per cm^3 of Flame Cases, Integrated Intensity of the Spectral Line for Atomic Emission, and Absorption Coefficient as Functions of Element and Line, Flame Type, Temperature, and the Total Partial Pressures of All Species of the Metal Present in the Flame Cases.

Two programs were used; one was designed for the alkali metals, and one was designed for the alkaline earths. They are very similar to each other and differ only in those arithmetic statements dealing with the expressions for the dissociation constants of the metal chlorides. For alkaline earths, this expression contains the partial pressure of the chlorine atom as a squared term; the alkali metal expression uses the corresponding term for the partial pressure of the chlorine atom to the first power. Both Fortran programs are given here in complete form but, since the programs are exactly the same in all other respects, only one discussion of the program will be given.

These programs are primarily designed to calculate the number of uncombined metal atoms present per cm^3 of the flame gases. From that value the intensity of emitted light in watts cm^{-2} $ster^{-1}$, I, and the absorption coefficient of the flame, k^0 in cm^{-1} are calculated. The former of these two is used in a later program of this work to calculate the signal, noise, signal-to-noise ratio, and optimum slit width; the latter will be useful if a similar study to this one is done on atomic absorption flame spectrometry.

The number of atoms in the flame depends upon the number introduced, P_T, and on the dissociation constants, or ionization constant, of the species competing with the atomic species. These constants depend upon the temperature and on the partial pressures of the gases (including electron pressure) involved in the formation of the competing species. The partial pressures of concern depend, in turn, on the flame type. Consequently the calculated values of N, I, and k^0 are produced by the programs in three dimensional arrays for which temperature, T, P_T, and flame type are the independent variables. The first value to be calculated by the program is the partial pressure of the atomic species of the metal, P_M. The technique used by the program for this calculation is that of successive approximation. Equation (30) for the alkaline earths is arranged in the following way:

$$2[(K_1K_2K_3K_4) + 4(K_2K_3K_4{P_T}^2) + (K_1K_3K_4P_O) + (K_1K_2K_4P_H) + (K_1K_2K_3P_{OH})]P_M + K_1K_2K_3K_4[(P_e')^2 + 4K_5P_M]^{1/2} = K_1K_2K_3K_4(P_e' + 2P_T) \quad . \qquad (46)$$

Equation (31) for the alkali metals is similarly rearranged:

$$2[(K_1K_2K_3K_4) + (K_2K_3K_4P_T) + (K_1K_3K_4P_O) + (K_1K_2K_4P_H) + (K_1K_2K_3P_{OH})]P_M + K_1K_2K_3K_4[(P_e')^2 + 4K_5P_M]^{1/2} = K_1K_2K_3K_4(P_e' + 2P_T) \quad . \qquad (47)$$

The coefficient of the first term on the left of each equation is set equal to the dummy term, A, for convenience. The left side of the equation is set equal to the dummy term, Q, and the right side is set equal to the dummy term, R. Thus for any arbitrary value of the term P_M if

$$\left|1 - Q/R\right| \leq .05 \quad , \qquad (48)$$

it is assumed that this value of P_M comes very close to satisfying the original equation (either (46) or (47)) and is therefore an acceptably correct value for P_M. When the arbitrarily chosen value of P_M does not satisfy the test of Equation (48), it is necessary to determine whether the approximation is too high or too low. This information is gained by another IF statement test. The R term is independent of P_M. Consequently if

$$Q > R \quad , \qquad (49)$$

it is because the approximated value of P_M is larger than it should be and vice versa. The complete procedure used is to take $P_M = 1/10\ P_T$ as the initial approximation; test this value for P_M with Equation (48); if it fails that test, an IF statement branching device using the inequality 49 causes the successive approximations to either increase or decrease as the program proceeds to an acceptable value of P_M. In either case, the succeeding approximations take tenfold jumps. The same IF statement using inequality 49 determines whether or not the tenfold jump has overshot the true value of P_M. When this is the case, the program backs up to the last previous approximated value of P_M and proceeds forward again by twofold jumps. The same test for overshooting is again employed, and when it does overshoot, the program again backs up to the immediately previous approximation and proceeds forward by 5 per cent jumps. A limit on the number of 5 per cent jumps was placed in the program to prevent some mechanical error from consuming too much computer time. If that limit should be reached, the program terminates and prints out information to that effect.

The value of N is calculated from the value of P_M by Equation (33) as described earlier. The value of I is calculated from the value of N by Equations (34) or (35), and k^o is calculated from the value of N by Equation (38); both calculations were also described earlier. The program uses terms which represent collections of the constants involved in Equations (34, 35, 37, and 38). The calculation of I involves the "intersection point" value of N.[32] This value is dependent on the temperature, and so a series of hand calculated values of the term including the "intersection point" N are fed in as data, one for each of the arbitrary temperature values used. These pieces of data are subscripted with the same symbol as the temperature data. The complete data required by either of these two programs consists of: a list of arbitrary values for temperature and P_T; the partial pressures, at each temperature and for each flame type, of hydrogen (H), oxygen (O), hydroxide (OH), and the electron pressure; the dissociation constants at each temperature for the chloride, monoxide, monohydride and monohydroxide; the ionization constant for the first stage of ionization at each temperature; values for the various collections of constant terms. In addition to these data, there are certain labeling directions for the printout required. The data for one line of one element constitutes a complete data deck for these programs. A GO TO 1 statement allows for the use of as many data decks as is desired to be used in the same computer run. The interpretation of the program terms is as follows:

EMIS(J,K,I)	Log of integrated intensity of the spectral line in watts cm^{-2} ster^{-1} calculated by the program.
ABS(J,K,I)	Log of absorption coefficient calculated by the program.
Z(J,K,I)	Log of the number of atoms of metal per cm^3 of flame gases calculated by the program.

XEMIS(J,K,I)	Integrated intensity of the spectral line in watts cm^{-2} ster^{-1} calculated by the program, I.
XABS(J,K,I)	Absorption coefficient calculated by the program, k^{o} cm^{-1}.
XZ(J,K,I)	Number of atoms of metal per cm^{3} of flame gases calculated by the program, N.
XKCL(I)	Dissociation constant of the metal chloride.
XKO(I)	Dissociation constant of the metal monoxide.
XKH(I)	Dissociation constant of the metal monohydride.
XKOH(I)	Dissociation constant of the metal monohydroxide.
XKE(I)	Ionization constant of the metal.
PTOT(K)	Total of the partial pressures of all the species of the metal present in the flame gases, P_T
T(I)	Arbitrary temperatures.
PO(J)	Partial pressure of oxygen (O) in the flame gases.
PH(J)	Partial pressure of hydrogen (H) in the flame gases.
POH(J)	Partial pressure of the neutral hydroxide (OH) in the flame gases.
PE	Partial pressure due to electrons in the flame gases.
L	Index limit of the subscript J which identifies the flame type.
M	Index limit of the subscript K which identifies the total of the partial pressures of all the species of the metal present in the flame gases.
N	Index limit of the subscript I which identifies the temperature.

PM	Dummy term for the partial pressure of the metal atom in the flame gases.
Q	Dummy term for the value of the left side of Equations (46) and (47).
R	Dummy term for the value of the right side of Equations (46) and (47).
A	Dummy term for the coefficient of P_M in the left side of Equations (46) and (47).
IKY	Dummy term to control the number of cycles of approximation used by the program.
SAM	Dummy term used in obtaining the antilog of EMIS(J,K,K).
BAM	Dummy term used in obtaining the antilog of Z(J,K,I).
DAM	Dummy term used in obtaining the antilog of ABS(J,K,I).
SPEK	Log $\log[\frac{2\sqrt{\ln 2}\,\lambda_o^2 g_u A_t \delta M_2^{1/2}}{7.15\text{x}10^{-7}\nu_o\sqrt{\pi}\,8\pi B_{(T)}})$
XXL	Log $\log[\frac{h\nu_o g_u A_t}{10^7 4\pi B_{(T)}}]$
EXC	Excitation energy in volts.
ZSA(I)	Log $\log[\frac{16\pi a\, 7.15\text{x}10^{-7}\nu_o T^{1/2}B_{(T)}}{M_2^{1/2}\sqrt{\ln 2}\, g_u A_t L \lambda_o^2}]$
ELEMT	Symbol of element used to label pages of output.
XLINE	Spectral line in angstroms used to label pages of output.
XFTP(J)	Flame type, used to label pages of output.

RATIO(J)	Ratio of fuel gas to oxygen, used to label pages of output.
TEMP(I)	Temperature values, used to label the tables in the output.

The composition of a complete data deck (assuming 8 temperatures, 8 P_T values, and 6 flame types) is as follows:

L M N

XKCL(1)	XKCL(2)	XKCL(3)	XKCL(4)
XKCL(5)	XKCL(6)	XKCL(7)	XKCL(8)
XKO(1)	XKO(2)	XKO(3)	XKO(4)
XKO(5)	XKO(6)	XKO(7)	XKO(8)
XKH(1)	XKH(2)	XKH(3)	XKH(4)
XKH(5)	XKH(6)	XKH(7)	XKH(8)
XKOH(1)	XKOH(2)	XKOH(3)	XKOH(4)
XKOH(5)	XKOH(6)	XKOH(7)	XKOH(8)
XKE(1)	XKE(2)	XKE(3)	XKE(4)
XKE(5)	XKE(6)	XKE(7)	XKE(8)
PTOT(1)	PTOT(2)	PTOT(3)	PTOT(4)
PTOT(5)	PTOT(6)	PTOT(7)	PTOT(8)
T(1)	T(2)	T(3)	T(4)
T(5)	T(6)	T(7)	T(8)
PO(1)	PO(2)	PO(3)	PO(4)
PO(5)	PO(6)	PH(1)	PH(2)
PH(3)	PH(4)	PH(5)	PH(6)
POH(1)	POH(2)	POH(3)	POH(4)
POH(5)	POH(6)	PE	SPEK

```
ZSA(1)        ZSA(2)         ZSA(3)         ZSA(4)
ZSA(5)        ZSA(6)         ZSA(7)         ZSA(8)
XKL           EXC
ELEMT  XLINE  TEMP(1)  TEMP(2)  TEMP(3)  TEMP(4)  TEMP(5)
TEMP(6)  TEMP(7)  TEMP(8)  XFTP(1) XFTP(2)  XFTP(3)
XFTP(4)  XFTP(5)  XFTP(6)  RATIO(1)  RATIO(2)  RATIO(3)
RATIO(4)  RATIO(5)  RATIO(6)
```

An example of the way the computed values are printed out is as follows:

```
NA  5890  HY/AR = 2/5
                       ABSORPTION COEFFICIENT
LOG OF P TOTAL   -10   -9   -8   ...   ...   ...
TEMPERATURE
  1800
  2000
  2200          (values of absorption coefficient)
   ...
   ...
   ...
```

The same pattern is used for printing out the values of numbers of atoms and intensity. There is one such table for a single flame type on each page.

The two Fortran programs, for the alkaline earths and the alkali metals, are as follows:

PROGRAM FOR ALKALINE EARTH METALS

```
      DIMENSION XKCL(10),XKO(10),XKH(10),XKOH(10),XKE(10),PT
     1OT(10),T(10),PO(15),PH(15),POH(15),Z(15,10,10),EMIS(15
     2,10,10),ZSA(10),ABS(15,10,10),XEMIS(15,10,10),XABS(15,
     310,10),XZ(15,10,10),TEMP(16),XFTP(15),RATIO(15)
    1 READ INPUT TAPE 5,6,L,M,N,(XKCL(I),I=1,N),(XKO(I),I=1,
     1N),XKH(I),I=1,N),(XKOH(I),I=1,N),(XKE(I),I=1,N),PTOT(K
     2),K=1,M),(T(I),I=1,N),(PO(J),J=1,L),(PH(J),J=1,L),(POH
     3(J),J=1,L),PE,SPEK,(ZSA(I),I=1,N),XKL,EXC
      READ INPUT TAPE 5,80,ELEMT,XLINE,(TEMP(I),I=1,N)
   80 FORMAT (2X,2A5,8F6.0)
      READ INPUT TAPE 5,100,(XFTP(J),J=1,L),(RATIO(J),J=1,L)
  100 FORMAT (2X,12A5)
      WRITE OUTPUT TAPE 6,7,L,M,N,(XKCL(I),I=1,N),(XKO(I),I=1,
     1N),XKH(I),I=1,N),(XKOH(I),I=1,N),(XKE(I),I=1,N),PTOT(K
     2),K=1,M),(T(I),I=1,N),(PO(J),J=1,L),(PH(J),J=1,L),(POH
     3(J),J=1,L),PE,SPEK,(ZSA(I),I=1,N),XKL,EXC
      WRITE OUTPUT TAPE 6,85,ELEMT,XLINE,(TEMP(I),I=1,N)
   85 FORMAT (1H0,2A5,8F6.0)
      WRITE OUTPUT TAPE 6,101,(XFTP(J),J=1,L),(RATIO(J),J=1,
     1L)
  101 FORMAT (1H0,12A5)
      DO 50 J=1,L
      DO 50 K=1,M
      DO 50 I=1,N
      IKY=1
      PM=0.10*PTOT(K)
      A=2.0*(XKCL(I)*XKO(I)*XKH(I)*XKOH(I)+4.0*XKO(I)*XKH(I)
     1*XKOH(I)*PTOT(K)+XKCL(I)*XKH(I)*XKOH(I)*PO(J)+XKCL(I)*
     2XKO(I)*XKOH(I)*PH(J)+XKCL(I)*XKO(I)*XKH(I)*POH(J))
      Q=A*PM+XKCL(I)*XKO(I)*XKH(I)*XKOH(I)*((PE*PE+4.00*XKE(
     1I)*PM)**0.5)
      R=XKCL(I)*XKO(I)*XKH(I)*XKOH(I)*(PE+2.00*PTOT(K))
      IF (ABSF(1.00-Q/R)-0.05)23,23,3
```

```
 3 IF (Q-R)5,5,26
 5 PM=10.00*PM
   Q=A*PM+XKCL(I)*XKO(I)*XKH(I)*XKOH(I)*((PE*PE+4.00*XKE(
  1I)*PM)**0.5)
   IF (ABSF(1.00-Q/R)-0.05)23,23,9
 9 IF (Q-R)5,11,11
11 PM=0.10*PM
13 PM=2.00*PM
   Q=A*PM+XKCL(I)*XKO(I)*XKH(I)*XKOH(I)*((PE*PE+4.00*XKE(
  1I)*PM)**0.5)
   IF (ABSF(1.00-Q/R)-0.05)23,23,15
15 IF (Q-R)13,17,17
17 PM=0.50*PM
19 PM=1.05*PM
   Q=A*PM+XKCL(I)*XKO(I)*XKH(I)*XKOH(I)*((PE*PE+4.00*XKE(
  1I)*PM)**0.5)
   IF (ABSF(1.00-Q/R)-0.05)23,23,21
21 IKY=IKY+1
   IF (IKY-20)19,22,22
22 WRITE OUTPUT TAPE 6,10,PM,Q,R,I,K,J
   GO TO 35
26 PM=0.10*PM
   Q=A*PM+XKCL(I)*XKO(I)*XKH(I)*XKOH(I)*((PE*PE+4.00*XKE(
  1I)*PM)**0.5)
   IF (ABSF(1.00-Q/R)-0.05)23,23,27
27 IF (R-Q)26,28,28
28 PM=10.00*PM
29 PM=0.50*PM
   Q=A*PM+XKCL(I)*XKO(I)*XKH(I)*XKOH(I)*((PE*PE+4.00*XKE(
  1I)*PM)**0.5)
   IF (ABSF(1.00-Q/R)-0.05)23,23,30
30 IF(R-Q)29,31,31
31 PM=2.00*PM
32 PM=0.95*PM
   Q=A*PM+XKCL(I)*XKO(I)*XKH(I)*XKOH(I)*((PE*PE+4.00*XKE(
  1I)*PM)**0.5)
```

```
      IF (ABSF(1.00-Q/R)-0.05)23,23,33
   33 IKY=IKY+1
      IF (IKY-20)32,34,34
   34 WRITE OUTPUT TAPE 6,12,PM,Q,R,I,K,J
      GO TO 35
   23 GO TO 35
   35 Z(J,K,I)=0.435*LOGF(PM/((1.38E-22)*T(I)))
      ABS(J,K,I)=SPEK+Z(J,K,I)-0.217*LOGF(T(I))
      IF(Z(J,K,I)-ZSA(I))40,40,45
   40 EMIS(J,K,I)=XKL+Z(J,K,I)-(5.05E3)*EXC/T(I)
      GO TO 50
   45 EMIS(J,K,I)=XKL+0.5*ZSA(I)+0.5*Z(J,K,I)-(5.05E3)*EXC/T
     1(I)
   50 CONTINUE
      DO 105 J=1,L
      DO 105 I=1,N
      DO 105 K=1,M
      SAM=EMIS(J,K,I)
      XEMIS(J,K,I)=10.**SAM
      BAM=Z(J,K,I)
      XZ(J,K,I)=10.**BAM
      DAM=ABS(J,K,I)
      XABS(J,K,I)=10.**DAM
  105 CONTINUE
      DO 113 J=1,L
      WRITE OUTPUT TAPE 6,114,ELEMT,XLINE,XFTP(J),RATIO(J)
      WRITE OUTPUT TAPE 6,115
      WRITE OUTPUT TAPE 6,118
      DO 107 I=1,N
      WRITE OUTPUT TAPE 6,119,TEMP(I),(XZ(J,K,I),K=1,M)
  107 CONTINUE
      WRITE OUTPUT TAPE 6,114,ELEMT,XLINE,XFTP(J),RATIO(J)
      WRITE OUTPUT TAPE 6,116
      WRITE OUTPUT TAPE 6,118
      DO 109 I=1,N
      WRITE OUTPUT TAPE 6,119,TEMP(I),(XEMIS(J,K,I),K=1,M)
```

```
10   CONTINUE
     WRITE OUTPUT TAPE 6,114,ELEMT,XLINE,XFTP(J),RATIO(J)
     WRITE OUTPUT TAPE 6,117
     WRITE OUTPUT TAPE 6,118
     DO 111 I=1,N
     WRITE OUTPUT TAPE 6,119,TEMP(I),(XABS(J,K,I),K=1,M)
 111 CONTINUE
 113 CONTINUE
     GO TO 1
   6 FORMAT (3I10/(4E15.3))
   7 FORMAT (1H0,3I10/(4E15.3))
  10 FORMAT (1X,11HPM IS SMALL,3E12.3,3I6)
  12 FORMAT (1X,11HPM IS LARGE,3E12.3,3I6)
 114 FORMAT (1H1,4X,4A5)
 115 FORMAT (1H0,40X,35HNUMBER OF ATOMS PER CC OF FLAME GAS
    1)
 116 FORMAT (1H0,42,30HINTENSITY IN WATTS/SQ CM,STER.)
 117 FORMAT (1H0,46X,22HABSORPTION COEFFICIENT)
 118 FORMAT (1H0,5X,14HLOG OF P TOTAL,8X,3H-10,10X,2H-9,10X
    1,2H-8,10X,2H-7,10X,2H-6,10X,2H-5,10X,2H-410X,2H-3//6X,
    211HTEMPERATURE)
 119 FORMAT (1H0,8X,1F5.0,10X,8E12.2)
     END
```

PROGRAM FOR ALKALI METALS

```
     DIMENSION XKCL(10),XKO(10),XKH(10),XKOH(10),XKE(10),PT
    1OT(10),T(10),PO(15),PH(15),POH(15),Z(15,10,10),EMIS(15
    2,10,10),ZSA(10),ABS(15,10,10),XEMIS(15,10,10),XABS(15,
    310,10),XZ(15,10,10),TEMP(16),XFTP(15),RATIO(15)
   1 READ INPUT TAPE 5,6,L,M,N,(XKCL(I),I=1,N),(XKO(I),I=1,
    1N),XKH(I),I=1,N),(XKOH(I),I=1,N),(XKE(I),I=1,N),PTOT(K
    2),K=1,M),(T(1),I=1,N),(PO(J),J=1,L),(PH(J),J=1,L),(POH
```

```
     3(J),J=1,L),PE,SPEK,(ZSA(I),I=1,N),XKL,EXC
      READ INPUT TAPE 5,80,ELEMT,XLINE,(TEMP(I),I=1,N)
   80 FORMAT (2X,2A5,8F6.0)
      READ INPUT TAPE 5,100,(XFTP(J),J=1,L),(RATIO(J),J=1,L)
  100 FORMAT (2X,12A5)
      WRITE OUTPUT TAPE 6,7,L,M,N,(XKCL(I),I=1,N),(XKO(I),I=1,
     1N),XKH(I),I=1,N),(XKOH(I),I=1,N),(XKE(I),I=1,N),PTOT(K
     2),K=1,M),(T(I),I=1,N),(PO(J),J=1,L),(PH(J),J=1,L),(POH
     3(J),J=1,L),PE,SPEK,(ZSA(I),I=1,N),XKL,EXC
      WRITE OUTPUT TAPE 6,85,ELEMT,XLINE,(TEMP(I),I=1,N)
   85 FORMAT (1H0,2A5,8F6.0)
      WRITE OUTPUT TAPE 6,101,(XFTP(J),J=1,L),(RATIO(J),J=1,
     1L)
  101 FORMAT (1H0,12A5)
      DO 50 J=1,L
      DO 50 K=1,M
      DO 50 I=1,N
      IKY=1
      PM=0.10*PTOT(K)
      A=2.0*(XKCL(I)*XKO(I)*XKH(I)*XKOH(I)+     XKO(I)*XKH(I)
     1*XKOH(I)*PTOT(K)+XKCL(I)*XKH(I)*XKOH(I)*PO(J)+XKCL(I)*
     2XKO(I)*XKOH(I)*PH(J)+XKCL(I)*XKO(I)*XKH(I)*POH(J))
      Q=A*PM+XKCL(I)*XKO(I)*XKH(I)*XKOH(I)*((PE*PE+4.00*XKE(
     1I)*PM)**0.5)
      R=XKCL(I)*XKO(I)*XKH(I)*XKOH(I)*(PE+2.00*PTOT(K))
      IF (ABSF(1.00-Q/R)-0.05)23,23,3
    3 IF (Q-R)5,5,26
    5 PM=10.00*PM
      Q=A*PM+XKCL(I)*XKO(I)*XKH(I)*XKOH(I)*((PE*PE+4.00*XKE(
     1I)*PM)**0.5)
      IF (ABSF(1.00-Q/R)-0.05)23,23,9
    9 IF (Q-R)5,11,11
   11 PM=0.10*PM
   13 PM=2.00*PM
      Q=A*PM+XKCL(I)*XKO(I)*XKH(I)*XKOH(I)*((PE*PE+4.00*XKE(
     1I)*PM)**0.5)
   IF (ABSF(1.00-Q/R)-0.05)23,23,15
15 IF (Q-R)13,17,17
17 PM=0.50*PM
19 PM=1.05*PM
   Q=A*PM+XKCL(ID*XKO(I)*XKH(I)*XKOH(I)*((PE*PE+4.00*XKE(
  1I)*PM)**0.5)
   IF (ABSF(1.00-Q/R)-0.05)23,23,21
21 IKY=IKY+1
   IF (IKY-20)19,22,22
22 WRITE OUTPUT TAPE 6,10,PM,Q,R,I,K,J
   GO TO 35
26 PM=0.10*PM
   Q=A*PM+XKCL(ID*XKO(I)*XKH(I)*XKOH(I)*((PE*PE+4.00*XKE(
  1I)*PM)**0.5)
   IF (ABSF(1.00-Q/R)-0.05)23,23,27
27 IF (R-Q)26,28,28
28 PM=10.00*PM
29 PM=0.50*PM
   Q=A*PM+XKCL(ID*XKO(I)*XKH(I)*XKOH(I)*((PE*PE+4.00*XKE(
  1I)*PM)**0.5)
   IF (ABSF(1.00-Q/R)-0.05)23,23,30
30 IF(R-Q)29,31,31
31 PM=2.00*PM
32 PM=0.95*PM
   Q=A*PM+XKCL(ID*XKO(I)*XKH(I)*XKOH(I)*((PE*PE+4.00*XKE(
  1I)*PM)**0.5)
   IF (ABSF(1.00-Q/R)-0.05)23,23,33
33 IKY=IKY+1
   IF (IKY-20)32,34,34
34 WRITE OUTPUT TAPE 6,12,PM,Q,R,I,K,J
   GO TO 35
23 GO TO 35
35 Z(J,K,I)=0.435*LOGF(PM/((1.38E-22)*T(I)))
   ABS(J,K,I)=SPEK+Z(J,K,I)-0.217*LOGF(T(I))
   IF(Z(J,K,I)-ZSA(I))40,40,45
40 EMIS(J,K,I)=XKL+Z(J,K,I)-(5.05E3)*EXC/T(I)
```

```
      GO TO 50
   45 EMIS(J,K,I)=XKL+0.5*ZSA(I)+0.5*Z(J,K,I)-(5.05E3)*EXC/T
     1(I)
   50 CONTINUE
      DO 105 J=1,L
      DO 105 I=1,N
      DO 105 K=1,M
      SAM=EMIS(J,K,I)
      XEMIS(J,K,I)=10.**SAM
      BAM=Z(J,K,I)
      XZ(J,K,I)=10.**BAM
      DAM=ABS(J,K,I)
      XABS(J,K,I)=10.**DAM
  105 CONTINUE
      DO 113 J=1,L
      WRITE OUTPUT TAPE 6,114,ELEMT,XLINE,XFTP(J),RATIO(J)
      WRITE OUTPUT TAPE 6,115
      WRITE OUTPUT TAPE 6,118
      DO 107 I=1,N
      WRITE OUTPUT TAPE 6,119,TEMP(I),(XZ(J,K,I),K=1,M)
  107 CONTINUE
      WRITE OUTPUT TAPE 6,114,ELEMT,XLINE,XFTP(J),RATIO(J)
      WRITE OUTPUT TAPE 6,116
      WRITE OUTPUT TAPE 6,118
      DO 109 I=1,N
      WRITE OUTPUT TAPE 6,119,TEMP(I),(XEMIS(J,K,I),K=1,M)
  109 CONTINUE
      WRITE OUTPUT TAPE 6,114,ELEMT,XLINE,XFTP(J),RATIO(J)
      WRITE OUTPUT TAPE 6,117
      WRITE OUTPUT TAPE 6,118
      DO 111 I=1,N
      WRITE OUTPUT TAPE 6,119,TEMP(I),(XABS(J,K,I),K=1,M)
  111 CONTINUE
  113 CONTINUE
      GO TO 1
    6 FORMAT (3I10/(4E15.3))
  7 FORMAT (1H0,3I10/(4E15.3))
 10 FORMAT (1X,11HPM IS SMALL,3E12.3,3I6)
 12 FORMAT (1X,11HPM IS LARGE,3E12.3,3I6)
114 FORMAT (1H1,4X,4A5)
115 FORMAT (1H0,40X,35HNUMBER OF ATOMS PER CC OF FLAME GAS
   1)
116 FORMAT (1H0,42,30HINTENSITY IN WATTS/SQ CM,STER.)
117 FORMAT (1H0,46X,22HABSORPTION COEFFICIENT)
118 FORMAT (1H0,5X,14HLOG OF P TOTAL,8X,3H-10,10X,2H-9,10X
   1,2H-8,10X,2H-7,10X,2H-6,10X,2H-5,10X,2H-410X,2H-3//6X,
   211HTEMPERATURE)
119 FORMAT (1H0,8X,1F5.0,10X,8E12.2)
    END
```

APPENDIX 3

Fortran Program for Calculating the Signal, Noise, and Signal-to-Noise Ratio in Atomic Emission Flame Spectrometry as Functions of Element and Line, Flame Type, Temperature, Slit Width, and the Total Partial Pressure of All Species of the Metal Present in the Flame Gases; and for Calculating the Optimum Slit Width as a Function of Element and Line, Flame Type, Temperature, and the Total Partial Pressure of All Species of the Metal Present in the Flame Gases.

This program uses the integrated intensity values, I, produced by the previous program, and it produces, for a given element and spectral line, two different types of calculated values. The first type is the optimum slit width which is a function of flame type, temperature, and P_T. The other type includes three calculated values, signal, noise, and signal-to-noise ratio, and is a function of four different variables: flame type, temperature, P_T, and slit width.

The calculation of the optimum slit width uses Equation (18) rearranged to include substitutions according to Equations (12), (13), and (14) is as follows:

$$2\Delta f K_c^{\,2} \psi^2 \left\{ [(I_c R_d)^2 W_o^{\,4}] + [(I_c R_d)^2 W_m + (I_c R_d I)] W^3 \right\} =$$

$$K_d \Delta f \left\{ K_c W_o [(I_c R_d W_m) + I] + 2 i_d \right\} \quad . \tag{50}$$

The program employs a series of successive approximations for the value of the optimum slit width, W_o. A testing device similar to that used in the previous program is employed to determine when an acceptable value of W_o is reached. The left side of Equation (50) is set equal to the dummy term, A, and the right side is set equal to the dummy term, B. Consequently when an approximated value of W_o satisfies the equation

$$|1 - A/B| \leq .05 \quad , \tag{51}$$

then that value of W_o is considered an acceptable value for W_o. The initial approximation for W_o is deliberately set low, 10 microns, and in the series the approximation is increased by small increments. The optimum slit width should correspond to the maximum in the curve of signal-to-noise ratio plotted against slit width. The maximum of such a curve is sometimes broad and flat. This approximation method for calculating the optimum slit width will only give the maximum of that curve and will not give any indication of how broad or how narrow the curve is. The optimum slit width, W_o, appears in term A raised to the third and fourth powers and so a small change in the W_o value used in the series of approximations is magnified in its effect on the rate of approach toward a W_o value that will satisfy Equation (50). This rapid approach brings on the possibility of overshooting the acceptable values of W_o unless the increments of increase are extremely small. However, extremely small increments will often consume a large amount of computer time. Therefore a moderately small increment is used, 5 microns, with a testing device to tell when the approximated value of W_o does overshoot the acceptable range. The testing device is similar to that used for the same purpose in the previous program. A low approximation for W_o will always cause A to be smaller than B because W_o is less than one cm and is raised to higher powers in A than it is in B. Because this approximation series starts low, A will be less than B at the beginning; if some approximated value of W_o is subsequently used which makes A larger than B, then the approximation series has overshot the acceptable range for W_o. The testing device, therefore, is simply to test whether or not A is larger than B for every step of the approximation. Whenever the test shows A to be larger than B, the approximation series terminates and a separate statement is printed out. In other words, for this particular set of values of the variables, the W_o value printed in the list of W_o values exceeds the acceptable value by less than 5 microns (the size of a single increase increment).

The calculation of the signal, noise, and signal-to-noise ratio involves no approximation and is simply a matter of evaluating Equations (15), (16), and (17) when a particular set of values for all of the terms is substituted into it.

The arrangement of the data must provide for including four different variables when a maximum of three subscripts per term is allowed. This is done by using separate data decks for each value of the fourth variable, the flame type. The data deck treatment can be somewhat simplified because some of the values to be used in the data deck are instrument parameters or properties of the element and line and are independent of flame type. It was therefore possible to use two different types of data decks in this program; one which contains only values that remain constant for a given element and line, and one which is controlled by a loop and which contains values that vary with each flame type as well as with element and line. A GO TO 1 statement makes it possible to use several complete sets of decks, one for each element and line, in the same computer run. The data used includes the same arbitrary values of temperature, P_T, and flame type used earlier and also an arbitrary set of slit widths. It also includes the values of terms representing collections of constants relating to instrument, element, line, and flame properties, as well as labels and directions for printing out the calculated values.

The scheme used in printing out the calculated values, so as to show the effect of all variables conveniently, places each different flame type on a separate page. The optimum slit width values then have only two variables remaining which are placed in a two dimension table on each page. The signal, noise, and signal-to-noise ratio have three remaining variables after the flame types are placed on separate pages. These are arranged in tables with two different levels of horizontal indexing and appear as one complete table per page.

The interpretation of the terms used in the program is as follows:

XI(J)	Intensity values in watts cm^{-2} $ster^{-1}$.
WO(J)	Optimum slit width in cm calculated by the program.
XW(K)	Arbitrary slit width values, in cm, to be used in calculating the signal, noise, and signal-to-noise ratio.
SIG(J,K)	Signal values, in amperes, calculated by the program.
RAC(J,K)	Noise values, in amperes, calculated by the program.
SNR(J,K)	Signal-to-noise ratio values calculated by the program.
SW(K)	Slit width values, in microns, used in labeling the tables of signal, noise, and signal-to-noise ratio.
D(J)	Log of P_T values used in labeling the tables of signal, noise, and signal-to-noise ratio.

C(JK)	Temperature values used in labeling the tables of signal, noise, and optimum slit width.
ELEMT	Element symbol to label a page of tables.
XLINE	Wavelength of the line, in Angstroms, to label a page of tables.
XFTP	Description of the flame type used to label a page of tables.
RATIO	Description of the fuel to oxygen ratio used to label a page of tables.
I	Index limit of subscript J identifying intensity values.
M	Index limit of subscript K identifying arbitrary slit width values.
KJ	Index limit of subscript JK which is used to select the proper temperature labels in printing the tables of signal and of noise.
L1,L2,L3,L4	Index limits used to select proper temperature values in printing tables of signal-to-noise ratio.
N1,N2,N3,N4	Values of temperature used in labeling the signal-to-noise ratio.
	tables
XKD	k_d
XKC	k_c
XDQ	Δf
XID	i_d
XWM	W_m
NN,NL	Index limits controlling the number of separate flame type data decks to be read into the computer.
XRD	R_d

XP	ψ
XIC	I_c

The composition of a complete set of data decks for a single element and spectral line, assuming 8 values of slit width and the same number of other values as were used in the previous program, is as follows:

(Deck of values that are independent of flame type)

I M KJ ELEMT XLINE SW(1) SW(2) SW(3) SW(4) SW(5)
SW(6) SW(7) SW(8) D(1) D(2) D(3) D(4) D(5) D(6)
D(7) D(8) D(9) D(10) D(11) D(12) D(13) D(14) D(15)
D(16) D(17) D(18) D(19) D(20) D(21) D(22) D(23)
D(24) D(25) D(26) D(27) D(28) D(29) D(30) D(31)
D(33) D(34) D(35) D(36) D(37) D(38) D(39) D(40)
D(41) D(42) D(43) D(44) D(45) D(46) D(47) D(48)
D(49) D(50) D(51) D(52) D(53) D(54) D(55) D(56)
D(57) D(58) D(59) D(60) D(61) D(62) D(63) D(64)
XKD XKC XDQ XID XWM XW(1)
XW(2) XW(3) XW(4) XW(5) XW(6) XW(7)
XW(8) C(1) C(2) C(3) C(4) C(5)
C(6) C(7) C(8) XRD

(control card governing the number of flame type decks to be used)

NL

(flame type deck)

```
XIC     XP      XI(1)   XI(2)   XI(3)   XI(4)
XI(5)   XI(6)   XI(7)   XI(8)   XI(9)   XI(10)
XI(11)  XI(12)  XI(13)  XI(14)  XI(15)  XI(16)
XI(17)  XI(18)  XI(19)  XI(20)  XI(21)  XI(22)
XI(23)  XI(24)  XI(25)  XI(26)  XI(27)  XI(28)
XI(29)  XI(30)  XI(31)  XI(32)  XI(33)  XI(34)
XI(35)  XI(36)  XI(37)  XI(38)  XI(39)  XI(40)
XI(41)  XI(42)  XI(43)  XI(44)  XI(45)  XI(46)
XI(47)  XI(48)  XI(49)  XI(50)  XI(51)  XI(52)
XI(53)  XI(54)  XI(55)  XI(56)  XI(57)  XI(58)
XI(59)  XI(60)  XI(61)  XI(62)  XI(63)  XI(64)
```

An example of the form in which the calculated values of optimum slit width are printed out:

```
ATOMIC EMISSION
NA   5890 AC/OX = 2/5
                           OPTIMUM SLIT WIDTH IN CM
LOG OF P TOTAL      -10     -9     -8     ...     ...     ...
  TEMPERATURE
    1800
    2000
    2200
                            (Values of optimum slit width)
     ...
     ...
     ...
```

An example of the form in which the calculated values of signal, noise and signal-to-noise ratio are printed out. There is room for complete sets of values for four temperature values on each page.

```
ATOMIC EMISSION
NA   5890   AC/OX = 2/5
                            SIGNAL TO NOISE RATIO
SLIT WIDTH IN MICRONS   30.    50.    70.    ...     ...     ...
TEMPERATURE      LOG P TOTAL
2400                -10
                    - 9
                    - 8
                    ..  (values of signal-to-noise ratio)
                    ..
                    ..
2600                -10
                    - 9
                    - 8
                    ..
                    ..
                    ..
```

The complete Fortran program is as follows:

```
   DIMENSION XI(64),WO(64),XW(8),SNR(64,8),C(8),SW(16),D(
  1128),SIG(64,8),RAC(64,8)
 1 READ INPUT TAPE 5,90,I,M,KJ,ELEMT,XLINE,(SW(K),K=1,M),
  1(D(J),J=1,I)
   READ INPUT TAPE 5,92,XKD,XKC,XDQ,XID,XWM,(XW(K),K=1,M)
  1,(C(JK),JK=1,KJ),XRD
   WRITE OUTPUT TAPE 6,94,I,M,KJ,ELEMT,XLINE,(SW(K),K=1,M
  1),(D(J),J=1,I)
   WRITE OUTPUT TAPE 6,96,XKD,XKC,XDQ,XID,XWM,(XW(K),K=1,
  1M),(C(JK),JK=1,KJ),XRD
90 FORMAT (3I4,2A5,10F5.0/(2X,14F5.0))
92 FORMAT (6E12.2)
94 FORMAT (1H1,3I4,2A5,10F5.0/(2X,14F5.0))
96 FORMAT (1H0/(2X,6E12.2))
   READ INPUT TAPE 5,102,NL
   DO 65 NN=1,NL
   READ INPUT TAPE 5,103,L1,L2,L3,L4,N1,N2,N3,N4,XFTP,RAT
  1IO,XIC,XP,(XI(J),J=1,I)
   WRITE OUTPUT TAPE 6,104,L1,L2,L3,L4,N1,N2,N3,N4,XFTP,R
  1ATIO,XIC,XP,(XI(J),J=1,I)
   DO 40 J=1,I
   IKY=1
   Q=1.0E-3
   A=(2.0*XDQ*((XKC*XP)**2.0)*((((XIC*XRD)**2.0)*(Q**4.0)
  1)+(((XWM*((XIC*XRD)**2.0))+(XIC*XRD*XI(J)))*(Q**3.0)))
  2)
   B=(XKD*XDQ*((XKC*Q*((XIC*XRD*XWM)+XI(J)))+(2.0*XID)))
   IF(ABSF(1.00-A/B)-0.05)39,39,20
20 IF(A-B)25,22,22
22 WRITE OUTPUT TAPE 6,105,J,Q,A,B
23 GO TO 39
25 Q=Q+5.E-4
   A=(2.0*XDQ*((XKC*XP)**2.0)*((((XIC*XRD)**2.0)*(Q**4.0)
  1)+(((XWM*((XIC*XRD)**2.0))+(XIC*XRD*XI(J)))*(Q**3.0)))
  2)
   B=(XKD*XDQ*((XKC*Q*((XIC*XRD*XWM)+XI(J)))+(2.0*XID)))
```

```
      IF(ABSF(1.00-A/B)-0.05)39,39,27
 27   IKY=IKY+1
      IF (IKY-200)20,29,29
 29   WRITE OUTPUT TAPE 6,106,J,Q,A,B
 30   GO TO 39
 39   WO(J)=Q
 40   CONTINUE
      WRITE OUTPUT TAPE 6,107,ELEMT,XLINE,XFTP,RATIO
      DO 50 JK=1,KJ
      LJ=JK*8-7
      JJ=JK*8
      WRITE OUTPUT TAPE 6,108,C(JK),(WO(J),J=LJ,JJ )
 50   CONTINUE
      DO 60 J=1,I
      DO 60 K=1,M
      SIG(J,K)=XKC*XW(K)*XI(J)
      RAC(J,K)=((XDQ*((XKD*(XID+(XKC*XW(K)*((XIC*XRD*(XW(K)+
     1XWM))+XI(J))))))+((XKC*XW(K)*(XP*XIC*XRD*(XW(K)+XWM)+(X
     2P*XI(J)))))**2)))**.5)
      SNR(J,K)=SIG(J,K)/RAC(J,K)
 60   CONTINUE
      WRITE OUTPUT TAPE 6,109,ELEMT,XLINE,XFTP,RATIO,(SW(K),
     1K=1,M)
      LJ=L1*8-7
      JJ=L1*8
      LL=L2*8-7
      KK=L2*8
      MM=L3*8-7
      NK=L3*8
      KM=L4*8-7
      KN=L4*8
      WRITE OUTPUT TAPE 6,110,N1,(D(J),(SNR(J,K),K=1,M),J=LJ
     1,JJ)
      WRITE OUTPUT TAPE 6,110,N2,(D(J),(SNR(J,K),K=1,M),J=LL
     1,KK)
      WRITE OUTPUT TAPE 6,110,N3,(D(J),(SNR(J,K),K=1,M),J=MM
     1,NK)
      WRITE OUTPUT TAPE 6,110,N4,(D(J),(SNR(J,K),K=1,M),J=KM
     1,KN)
      WRITE OUTPUT TAPE 6,111,ELEMT,XLINE,XFTP,RATIO,(SW(K),
     1K=1,M)
      DO 61 JK=1,4
      LJ=JK*8-7
      JJ=JK*8
      WRITE OUTPUT TAPE 6,112,C(JK),(D(J),(SIG(J,K),K=1,M),J
     1=LJ,JJ)
   61 CONTINUE
      WRITE OUTPUT TAPE 6,111,ELEMT,XLINE,XFTP,RATIO,(SW(K),
     1K=1,M)
      DO 62 JK=5,8
      LJ=JK*8-7
      JJ=JK*8
      WRITE OUTPUT TAPE 6,112,C(JK),(D(J),(SIG(J,K),K=1,M),J
     1=LJ,JJ)
   62 CONTINUE
      WRITE OUTPUT TAPE 6,113,ELEMT,XLINE,XFTP,RATIO,(SW(K),
     1K=1,M)
      DO 63 JK=1,4
      LJ=JK*8-7
      JJ=JK*8
      WRITE OUTPUT TAPE 6,112,C(JK),(D(J),(RAC(J,K),K=1,M),J
     1=LJ,JJ)
   63 CONTINUE
      WRITE OUTPUT TAPE 6,113,ELEMT,XLINE,XFTP,RATIO,(SW(K),
     1K=1,M)
      DO 64 JK=5,8
      LJ=JK*8-7
      JJ=JK*8
      WRITE OUTPUT TAPE 6,112,C(JK),(D(J),(RAC(J,K),K=1,M),J
     1=LJ,JJ)
   64 CONTINUE
   65 CONTINUE
```

```
      GO TO 1
  102 FORMAT (1I12)
  103 FORMAT (8I6/2A5/(6E12.2))
  104 FORMAT (1H2,8I6/4X,2A5/(6E12.2))
  105 FORMAT (1H0,4X,51HW-ZERO OVERSHOT TRUE VALUE BY LESS T
     1HAN  5  MICRONS/4X,I15,3E12.2)
  106 FORMAT (1H0,4X,38HW-ZERO IS GREATER THAN ONE MILLIMETE
     1R /4X,I15,3E12.2)
  107 FORMAT (1H1,3X,15HATOMIC EMISSION/4X,4A5///49X,24HOPTI
     1MUM SLIT WIDTH IN CM///5X,14HLOG OF P TOTAL,8X,3H-10,1
     10X,2H-9,10X,2H-8,10X,2H-7,10X,2H-6,10X,2H-5,10X,2H-4,1
     30X,2H-3//9X,11HTEMPERATURE)
  108 FORMAT (1H0,11X,F6.0,8E12.2)
  109 FORMAT (1H1,3X,15HATOMIC EMISSION//4X,4A5///48X,21HSIG
     1NAL  TO NOISE RATIO///4X,21HSLIT WIDTH IN MICRONS,2X,F
     25.0,7X,F5.0,7X,F5.0,7X,F5.0,7X,F5.0,7X,F5.0,7X,F5.0,
     37X,F5.0,//4X,24HTEMPERATURE  LOG P TOTAL)
  110 FORMAT (1H0,7X,I5/(17X,F5.0,2X,8E12.2))
  111 FORMAT (1H1,3X,15HATOMIC EMISSION//4X,4A5///51X,14HSIG
     1NAL IN AMPS///4X,21HSLIT WIDTH IN MICRONS,2XF500,7X,F5
     20,7X,F5.3,7X,F5.0,7X,F5.0,7X,F5.0,7X,F5.0,7X,F5.0//4X,
     324HTEMPERATURE  LOG P TOTAL)
  112 FORMAT (1H0,7X,F6.0/(17X,F5.0,2X,8E12.2))
  113 FORMAT (1H1,3X,15HATOMIC EMISSION//4X,4A5///52X,13HNOI
     1SE IN AMPS///4X,21HSLIT WIDTH IN MICRONS,2X,F5.0,7X,F5
     1.0,7X,F5.0,7X,F5.0,7X,F5.0,7X,F5.0,7X,F5.0//4X,24HTEMP
     1ERATURE LOG P TOTAL)
       END
```

APPENDIX 4

Literature Sources for Values of Parameters Used in Calculation of Integrated Intensity, Absorption Coefficient, and Signal-to-Noise Ratio.

A	area of slit, cm^2	Vickers[24]
a	classical damping factor	Hinnov[10]
A_t	transition probability, sec^{-1}	Corliss and Bozman[5]
B	factor characteristic of photodetector surface	Vickers[24]
$B(T)$	partition function	Landolt-Börnstein[18]
E_u	excitation energy of state u, electron volts	Landolt-Börnstein[18]
F	focal length of collimator, cm	Vickers[24]
g_u	statistical weight of upper u state	Landolt-Börnstein[18]
H	height of slit	Vickers[24]
R_d	reciprocal linear dispersion, $m\mu\ cm^{-1}$	Vickers[24]
T_f	transmission factor	Vickers[24]
W_m	minimum resolving power slit width, $m\mu$	Herrmann and Alkemade[8]
δ	factor to account for broadening other than Doppler broadening	Poesner[21]

LITERATURE CITED

1. Alkemade, C. T. J., "Excitation and Related Phenomena in Flames," "Proceedings of the Xth Colloquium Spectroscopicm Internationale," E. R. Lippincott, M. Margoshes, editors, Spartan Books, Washington, 1963.

2. Broderson, S., *J. Opt. Soc. Am.* *43*, 877 (1953).

3. Broderson, S., *ibid.*, *44*, 22 (1954).

4. Bulewicz, E. M., Sugden, J. M., *Trans. Faraday Soc.* *55*, 720 (1959).

5. Corliss, C. H., Bozman, W. R., "Experimental Transition Probabilities for Spectral Lines of Seventy Elements," National Bureau of Standards Monograph 53, 1962.

6. Gaydon, A. G., Wolfhard, H. G., "Flames, Their Structure Radiation and Temperature," Chapman and Hall, London, 1960.

7. Gilbert, P. T., Jr., "Analytical Flame Photometry: New Developments," Symposium on Spectroscopy, American Society for Testing Materials, Special Technical Publications, No. 269, 1960.

8. Herrmann, R., Alkemade, C. T. J., "Flammenphotometrie," 2nd ed., Springer Verlag, Berlin, 1960. "Chemical Analysis by Flame Photometry," P.T. Gilbert, translator, Wiley, New York, 1963.

9. Herzberg, G., "Molecular Spectra and Molecular Structure. I. Spectra of Diatomic Molecules," 2nd ed., Van Nostrand, New York, 1950.

10. Hinnov, E., Kohn, H., *J. Opt. Soc. Am.* *47*, 156 (1957).

11. Hottel, H. C., Williams, G. C., Satterfield, C. N., "Thermodynamic Charts for Combustion Processes," John Wiley, New York, 1949.

12. Huldt, L., Lagerquist, A., *Arkiv för Fysik*, *2*, 333 (1950).

13. James, C. G., Sugden, T. M., Nature 171, 428 (1953).

14. James, C. G., Sugden, T. M., ibid., 175, 333 (1955).

15. James, C. G., Sugden, T. M., Proc. Roy. Soc. (London) A248, 238 (1958).

16. "JANAF Interim Thermochemical Tables," Dow Chemical Co., Midland, Mich., 1960.

17. Jones, H. C., Fisher, D. J., Kelley, M. T., 5th Conference on "Analytical Chemistry in Nuclear Reactor Technology," Gatlinburg, Tenn., Oct., 1961, Pamphlet No. T.I.D.-7629, p. 31.

18. Landolt-Börnstein, "Atom- und Molekularphysik," Vol. I, Part I, Springer Verlag, Berlin, 1950.

19. Lion, K. S., "Instrumentation in Scientific Research," McGraw-Hill Book Co., New York, 1961.

20. Mavrodineanu, R., Boiteux, H., "L'analyse spectrale quantitative par la flamme," Masson et Cle., Paris, 1954.

21. Poesner, D. W., Australian J. Phys. 17, 184 (1959).

22. Sugden, T. M., Wheeler, R. C., Discussions Faraday Soc., 19, 76 (1955).

23. Vickers, T. J., unpublished data, University of Florida, Gainesville, Florida.

24. Vickers, T. J., Ph.D. Dissertation, University of Florida, Gainesville, Florida, 1964.

25. Vickers, T. J., unpublished data, University of Florida, Gainesville, Florida.

26. Winefordner, J. D., Appl. Spectr. 17, 109 (1963).

27. Winefordner, J. D., Mansfield, C. T., Vickers, T. J., Anal. Chem. 35, 1607 (1963).

28. Winefordner, J. D., Mansfield, C. T., Vickers, T. J., ibid., 35, 1611 (1963).

29. Winefordner, J. D., Vickers, T. J., ibid., 36, 1939 (1964).

30. Winefordner, J. D., Vickers, T. J., *ibid.*, *36*, 1947 (1964).

31. Winefordner, J. D., Veillon, C., *ibid.*, *37*, 416 (1965).

32. Winefordner, J. D., Vickers, T. J., Remington, L. D., *ibid.*, *37*, 1216 (1965).

33. Zaer, A. R., Ph.D. thesis, Paris, 1935.

BIOGRAPHICAL SKETCH

Lloyd Dean Remington was born December 29, 1919, at Jackson, Michigan. In June, 1937, he was graduated from St. Petersburg Senior High School, St. Petersburg, Florida. He received the degree of Bachelor of Science in chemistry from the University of Michigan in June, 1942. From 1942, until 1946, he was employed as a chemist by the Buick Motor Division of General Motors Corporation. In 1946, he accepted a teaching position with the Pinellas County, Florida, Board of Public Instruction and taught chemistry and other sciences in that school system until 1965. By attending summer terms he received the degree of Master of Education from the University of Florida in 1954. He spent a sabbatical leave at Cornell University during the 1961-1962 academic year and received the degree of Master of Science Teaching in 1962, from Cornell University. He took a year's leave of absence (1963-64) during which he enrolled in the Graduate School of the University of Florida; he was also a graduate teaching assistant at the university during that year. In August, 1965, he became an Assistant Professor of chemistry at Asheville-Biltmore College in Asheville, North Carolina.

He is married to the former Violet Gertrude Giroux and is the father of four daughters. He is a member of the American Chemical Society, Alpha Chi Sigma fraternity and the Grace Covenant Presbyterian Church in Asheville, North Carolina. He has attended National Science Foundation summer and academic year institutes for secondary school teachers at the University of North Carolina (1957) and Cornell University (1961-62), respectively. He also received the National Science Foundation Summer Fellowship for Secondary School Teachers for six summers (1959-64) and spent this time studying at the University of Florida. In the summer of 1965, he was included in a National Science Foundation Research Participation Program at the University of Florida and was granted an academic year extension of that program. He was given a Shell Merit fellowship at Cornell University (1956) and was awarded the Florida Section of the American Chemical Society Award for the Outstanding High School Chemistry Teacher (1961).

This dissertation was prepared under the direction of the chairman of the candidate's supervisory committee and has been approved by all members of that committee. It was submitted to the Dean of the College of Arts and Sciences and to the Graduate Council, and was approved as partial fulfillment of the requirements for the degree of Doctor of Philosophy.

April 23, 1966

E. Ruffin Jones
Dean, College of Arts and Sciences

Dean, Graduate School

Supervisory Committee:

J. D. Winefordner
Chairman

W S Bray

R C Stoufer

W. M. Jones

L A Arnold